



Contents lists available at ScienceDirect

# Journal of Power Sources

journal homepage: [www.elsevier.com/locate/jpowsour](http://www.elsevier.com/locate/jpowsour)



## Review

# Review on recent progress of nanostructured anode materials for Li-ion batteries



Subrahmanyam Goriparti <sup>a,b</sup>, Ermanno Miele <sup>a,b</sup>, Francesco De Angelis <sup>a</sup>, Enzo Di Fabrizio <sup>c</sup>, Remo Proietti Zaccaria <sup>a</sup>, Claudio Capiglia <sup>a,\*</sup>

<sup>a</sup> Istituto Italiano di Tecnologia, Department of Nanostructures, Via Morego 30, Genova I-16163, Italy

<sup>b</sup> University of Genova, Genova 16145, Italy

<sup>c</sup> King Abdullah University of Science and Technology (KAUST), Thuwal 23955, Saudi Arabia

## HIGHLIGHTS

- Recent progress of nanosized active anode materials has been reviewed.
- Shape and size control of nanosized active materials.
- Improved specific capacity, cycle life and rate capability of active materials.
- Anodes with conductive matrices showing superior rate capability and cyclability.

## ARTICLE INFO

### Article history:

Received 3 August 2013

Received in revised form

18 November 2013

Accepted 22 November 2013

Available online 22 January 2014

### Keywords:

Li-ion batteries

Anode materials

Nano-structures

Rechargeable batteries

## ABSTRACT

This review highlights the recent research advances in active nanostructured anode materials for the next generation of Li-ion batteries (LIBs). In fact, in order to address both energy and power demands of secondary LIBs for future energy storage applications, it is required the development of innovative kinds of electrodes. Nanostructured materials based on carbon, metal/semiconductor, metal oxides and metal phosphides/nitrides/sulfides show a variety of admirable properties for LIBs applications such as high surface area, low diffusion distance, high electrical and ionic conductivity. Therefore, nanosized active materials are extremely promising for bridging the gap towards the realization of the next generation of LIBs with high reversible capacities, increased power capability, long cycling stability and free from safety concerns. In this review, anode materials are classified, depending on their electrochemical reaction with lithium, into three groups: intercalation/de-intercalation, alloy/de-alloy and conversion materials. Furthermore, the effect of nanoscale size and morphology on the electrochemical performance is presented. Synthesis of the nanostructures, lithium battery performance and electrode reaction mechanisms are also discussed. To conclude, the main aim of this review is to provide an organic outline of the wide range of recent research progresses and perspectives on nanosized active anode materials for future LIBs.

© 2013 The Authors. Published by Elsevier B.V. Open access under CC BY license.

## 1. Introduction

The research community is currently engaging in profuse efforts to achieve effective energy storage strategies which are the key for the exploitation of alternative energy and thus for the replacement of fossil fuels and traditional energy sources [1]. In this regard, rechargeable Li-ion batteries (LIBs) play a significant role due to

their high gravimetric and volumetric energy, high power density, long cycle life and low self-discharge property [2–9]. Furthermore, they have proved to be the most efficient energy storage strategy for a wide range of portable devices like cellular phones, laptops and digital electronics [10–16]. However, the employment of Li-ion batteries in hybrid electric vehicles (HEV), plug in hybrid electric vehicles (PHEV) and pure electric vehicles (PEV), needs from two to five times more energy density than the present lithium batteries technology can offer (150 Wh/kg) [17]. The increase of the energy density of lithium batteries can be achieved by either using high voltage cathode active materials as electrodes or by developing high capacity anode and cathode electrode materials. One of the main hindrances to design high voltage cathode in LIBs is

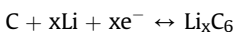
\* Corresponding author.

E-mail addresses: [claudio.capiglia@iit.it](mailto:claudio.capiglia@iit.it), [claudio@mvc.biglobe.ne.jp](mailto:claudio@mvc.biglobe.ne.jp) (C. Capiglia).

represented by the electrolyte decomposition that occurs at more than 4.2 V vs. Li/Li<sup>+</sup> [18–27]. Hence, the development of electrolyte with wider electrochemical window stability is also essential in the realization of the next generation of devices that will operate at higher cell potential with appropriate Li-ion conductivity. In this sense, remarkable research is still under progress to improve the performance of LIBs by using inorganic and organic based materials [2–9,28–35].

The common concept of present LIBs relies, at the cathode side, on transition metals oxides or phosphates active material (LiCoO<sub>2</sub>, LiMn<sub>2</sub>O<sub>4</sub>, LiCo<sub>1/3</sub>Mn<sub>1/3</sub>Ni<sub>1/3</sub>O<sub>2</sub>, LiFePO<sub>4</sub>, etc.), while graphite is commonly used as anode active material. Cathode and anode are separated by a membrane made of polypropylene/polyethylene filled with electrolyte which contains lithium salts (i.e. LiPF<sub>6</sub>) in alkyl organic carbonates such as ethylene, propylene, dimethyl carbonates at different ratio. The separator prevents the electrical contact between the electrodes and, at the same time, it allows the diffusion of Li-ions from cathode to anode during the charging and the reverse discharging process. The latter is defined as the flow of Li-ions from the anode to the cathode allowing the conversion of chemical energy into electrical energy. For example, the chemical reactions occurring in a typical LIB based on LiCoO<sub>2</sub> cathode are as follows:

Anode:



Cathode:



Active materials, in order to be considered suitable candidates for LIBs, should fulfil the requirements of reversible capacity, good ionic and electrical conductivity, long cycle life, high rate of lithium diffusion into active material and conclusively low cost and eco-compatibility.

The state-of-the-art for cathode materials is represented by LiCoO<sub>2</sub>, LiMn<sub>2</sub>O<sub>4</sub>, and LiFePO<sub>4</sub> [33–38], while graphite is definitely the most used anode [2–5] owing to its excellent features, such as flat and low working potential vs. lithium, low cost and good cycle life. However, graphite allows the intercalation (see Fig. 1) of only one Li-ion with six carbon atoms, with a resulting stoichiometry of LiC<sub>6</sub> and thus an equivalent reversible capacity of 372 mAh g<sup>-1</sup>. In addition, the diffusion rate of lithium into carbon materials is

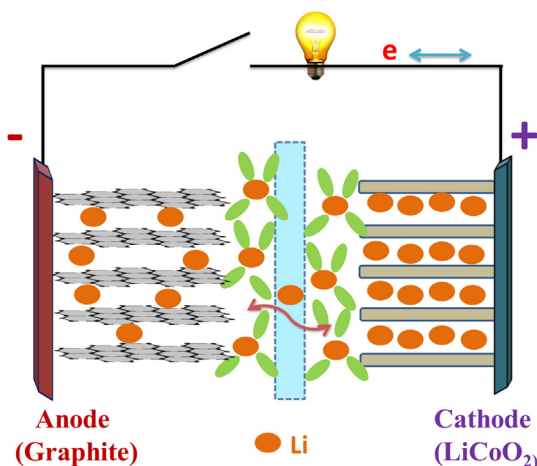


**Fig. 1.** Schematic representation of lithium insertion/de-insertion mechanism for current rechargeable lithium battery.

between 10<sup>-12</sup> and 10<sup>-6</sup> cm<sup>2</sup> s<sup>-1</sup> (for graphite it is between 10<sup>-9</sup> and 10<sup>-7</sup> cm<sup>2</sup> s<sup>-1</sup>), which results in batteries with low power density [39,40]. Hence, there is an urgency to replace graphite anodes to materials with higher capacity, energy and power density. Even though lithium metal holds one of the highest capacity among anode materials (3860 mAh g<sup>-1</sup>), safety issues prevent the use of lithium as anode material in secondary batteries. In fact, dendrites formation on the lithium metal can cause short circuit between anode and cathode [14,41,42].

Therefore, the path leading to LIBs with improved energy and power density has, as major challenge, the selection of suitable anode materials which can provide high capacity and ease diffusion of Li-ions into the anode, along with good cycling life and free from safety concerns (see Fig. 2).

Many efforts have been done in the investigation of both carbon and non-carbon materials for high performances and high capacity anode in LIBs. A short list must include: carbon nanotubes (1100 mAh g<sup>-1</sup>) [43], carbon nanofibers (450 mAh g<sup>-1</sup>) [44], graphene (960 mAh g<sup>-1</sup>) [45], porous carbon (800–1100 mAh g<sup>-1</sup>) [46], SiO (1600 mAh g<sup>-1</sup>) [47], silicon (4200 mAh g<sup>-1</sup>) [48], germanium (1600 mAh g<sup>-1</sup>) [49], tin (994 mAh g<sup>-1</sup>) [50] and transition metal oxides (500–1000 mAh g<sup>-1</sup>) [51–53]. Furthermore, metal sulphides, phosphides and nitrides [54–56] might be also considered for anodes purposes, in fact they possess specific capacity higher than 500 mAh g<sup>-1</sup>. However, high volume expansion, poor electron transport, capacity fading, and low coulombic efficiency as well, are the main limitations that have to be overcome before they can be used as effective anodes. In this sense, promising results and a bright perspective is offered by *nanostucturing* the above listed materials. Nano-size and tailored morphology represent the key feature capable of leading these innovative materials from being theoretically relevant to an effective technological breakthrough [57–60]. The expected advantages from using nanotechnology in LIBs can be listed as follow [56,61–64]:

- i) Realization of active materials with high surface to volume ratio, therefore intensification of the presence of active sites for lithium storage. This would result in a considerable increase of the specific capacity. Furthermore, the high surface area would imply a high contact area with the electrolyte, hence leading to high lithium-ion flux across the electrode/electrolyte interface.
- ii) Considering that some of the electrochemical reactions are hard to be triggered in bulk materials, shifting the anode research to the nanoscale would result in removing these limitations (for example βMnO<sub>2</sub>) [65].

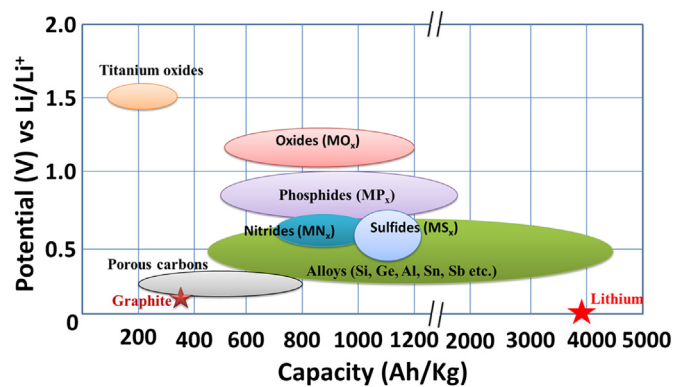


**Fig. 2.** Schematic illustration of active anode materials for the next generation of lithium batteries. Potential vs. Li/Li<sup>+</sup> and the corresponding capacity density are shown.

- iii) Improved lithium diffusion due to the reduction of its path length, hence batteries with enhanced power capability.
- iv) Higher electron transfer rates.

In the next sections we will discuss the state of the art of anode materials for LIBs, with particular emphasis on the recent nanotechnology research outcomes and outstanding results. For sake of simplicity, we will classify the discussed innovative anode materials in three main groups, depending on their Li-ion battery performances and reaction mechanism (see Table 1):

- 1) Intercalation/de-intercalation materials, such as carbon based materials, porous carbon, carbon nanotubes, graphene,  $TiO_2$ ,  $Li_4Ti_5O_{12}$ , etc;
- 2) Alloy/de-alloy materials such as Si, Ge, Sn, Al, Bi,  $SnO_2$ , etc;
- 3) Conversion materials like transition metal oxides ( $Mn_xO_y$ ,  $NiO$ ,  $Fe_xO_y$ ,  $CuO$ ,  $Cu_2O$ ,  $MoO_2$  etc.), metal sulphides, metal phosphides and metal nitrides ( $M_xX_y$ ; here X = S, P, N).

## 2. Insertion/de-insertion materials

### 2.1. Carbon based materials

Carbon-based materials with various consistencies and morphologies have been recognized as appropriate anode materials for LIBs due to their features, such as ease of availability, stability in thermal, chemical and electrochemical environment, low cost, and good lithium intercalation and de-intercalation reversibility [2–5,66]. These characteristics are quite important especially when considering that charged electrode materials, either delithiated cathodes or lithiated anodes, have the tendency to violently react with non-aqueous electrolytes at elevated temperatures. However, also at room temperature, side reactions can occur [66–69]. In particular, the lithium salt  $LiPF_6$  has the tendency of reacting with moisture resulting in the formation of HF. The produced HF would, in turn, cause the dissolution of any transition metal in the

electrodes and/or the surface erosion of the active materials, therefore leading to capacity decay upon charge–discharge cycling. The final result is the slow degradation of both the active electrode material and the electrolyte as well as the formation of a *thick* passive layer on the electrode surface during cycling. In particular, when it comes to anode, this layer is known as Solid Electrolyte Interface (SEI). In this regard, the use of carbon coating on the active materials can provide a way to mitigate the mentioned drawbacks. In fact, carbon shows an electrochemical activity towards the electrolyte only at very low potentials, and without any oxidation up to the cutoff voltage of the battery. Furthermore, high resistance to HF corrosion can be expected owing to the very good chemical stability of carbon. Finally, carbon coating can also prevent the surface oxidation of active materials in air, especially at the nano-scale level. In fact, nanostructured active materials present a high surface area which enhances the surface oxidation. For these reasons the carbon coating has the capability to greatly retard any surface degradation during storage and to strongly reduce the capacity fading upon charge–discharge cycling.

Some studies reporting the role of carbon coating on anode active materials for Li-ion batteries are here listed. For example, Zhang et al. directly observed the difference in the SEI formation between carbon coated and non-coated graphite anode [68]. The SEI film for carbon coated natural graphite spheres was found to be quite compact with a thickness from 60 nm to 150 nm, much thinner than the SEI film found on uncoated graphite spheres, showing thickness from 450 nm to 980 nm. The conclusion was that carbon coating can reduce the decomposition of the electrolyte and it can lead to the formation of a *thin* SEI on the electrode surface. Furthermore, it has been proved that after carbon coating the graphite surface, any direct contact of graphite with the electrolyte is prevented, therefore the decomposition of propylene carbonate is greatly reduced and the intercalation of electrolyte species (organic carbonates) into graphene layer is prevented [69,70]. The role of carbon coating on different kinds of active materials other than graphite has also been studied. For example, He et al. investigated the effect of carbon coating on

**Table 1**  
Most common anode materials used for lithium ion batteries.

Active anode material	Theoretical capacity ( $mAh g^{-1}$ ) [Reference]	Advantages	Common issues
<b>Insertion/de-insertion materials</b>			
A. Carbonaceous	200–600 [83–85]	➤ Good working potential	❖ Low coulombic efficiency
a. Hard carbons	1116 [91–94]	➤ Low cost	❖ High voltage hysteresis
b. CNTS	780/1116 [45]	➤ Good safety	❖ High irreversible capacity
c. Graphene			
B. Titanium oxides	175 [121]	➤ Extreme safety	❖ Very low capacity
a. $LiTi_4O_5$	330 [121]	➤ Good cycle life	❖ Low energy density
b. $TiO_2$		➤ Low cost	
		➤ High power capability	
<b>Alloy/de-alloy materials</b>			
a. Silicon	4212 [156]	➤ Higher specific capacities	❖ Large irreversible capacity
b. Germanium	1624 [191,192]	➤ High energy density	❖ Huge capacity fading
c. Tin	993 [61]	➤ Good safety	❖ Poor cycling
d. Antimony	660 [150]		
e. Tin oxide	790 [52]		
f. SiO	1600 [47]		
<b>Conversion materials</b>			
a. Metal oxides( $Fe_2O_3$ , $Fe_3O_4$ , $CoO$ , $Co_3O_4$ , $Mn_xO_y$ , $Cu_2O/CuO$ , $NiO$ , $Cr_2O_3$ , $RuO_2$ , $MoO_2/MoO_3$ etc.)	500–1200 [51–53, 56]	➤ High capacity	❖ Low coulombic efficiency
b. Metal phosphides/sulfides/nitrides ( $MX_y$ ; M = Fe, Mn, Ni, Cu, Co etc. and X = P, S, N)	500–1800 [54–56]	➤ High energy	❖ Unstable SEI formation
		➤ Low cost	❖ Large potential hysteresis
		➤ Environmentally compatibility	❖ Poor cycle life
		➤ High specific capacity	❖ Poor capacity retention
		➤ Low operation potential and Low polarization than counter oxides	❖ Short cycle life
			❖ High cost of production

$\text{Li}_4\text{Ti}_5\text{O}_{12}$  finding that it reduces the decomposition of the electrolyte when compared to uncoated  $\text{Li}_4\text{Ti}_5\text{O}_{12}$  [71] (for further information on LTO see section 2.2.1). Similarly, carbon coating of Silicon and Germanium was shown to improve the lithium-ion battery performance [72,73] (for further information on Si and Ge see sections 3.1 and 3.3, respectively). The importance of carbon coating on silicon surface has been examined in details by using FT-IR and X-ray photoelectronic spectroscopy [67]. In this study the authors observed that the absence of native oxide layer on silicon surface was prevented by carbon coating. In addition, the formation of silicon and carbon fluorides ( $\text{CF}_x$  and  $\text{SiF}_x$ ) into SEI was not found, meaning that the involvement of active materials (i.e. Silicon) into the SEI formation can be reduced/prevented through carbon coating. However, in this study the authors also reported about the formation of siloxane species in SEI for carbon coated silicon electrodes, otherwise absent when uncoated silicon electrodes were considered. Further examples on the role of carbon coating on anode active materials will be described in the next sections.

The variety of carbon based materials used as active anode in LIBs are classified into two categories, according to the degree of crystallinity and carbon atoms stacking [3,74]: i) SOFT carbon (graphitizable carbons) where crystallites are stacked almost in the same direction and ii) HARD carbon (non-graphitizable carbons) where crystallites have disordered orientation. In particular, the former is quite popular in the battery community. In fact, it shows an appropriate reversible capacity (i.e.  $350\text{--}370 \text{ mAh g}^{-1}$ ), long cycling life and good coulombic efficiency (more than 90%) [2,37,55,69,75,76]. The reaction mechanism between lithium and graphite, following an intercalation/de-intercalation process, has been extensively studied with various analytical techniques [77,78]. Among the types of commercially available graphite is worth mentioning Mesocarbon Microbead (MCMB), Mesophase-pitch-based carbon fibre (MCF), vapour grown carbon fibre (VGCF) and Massive Artificial Graphite (MAG). Despite their massive production and the relative low cost of the industrial processes, these classes of carbon materials have, as major issue, a low specific capacity (i.e.  $372 \text{ mAh g}^{-1}$ ), especially for applications such as HEV, PHEV or PEV. Hence, the use of graphitic carbon as anode is still limited to low power devices like mobile phones and laptops. Therefore, further advances in anode materials for lithium batteries are necessary to the development of competitive performance electric vehicles, smart electric grid systems and, in general, of portable high power consuming devices. One of the possible scenario involves the use of carbon base materials showing high capacity [37,79]. Presently, the research activity is strongly focused on porous carbon, carbon nanotubes (CNTs), nanofibers and graphene, as the most promising carbon based anode materials. The size reduction and the unique shape of these structures introduce novel properties that can substantially improve the energy storage capacity in LIBs [37,42–45,73,80]. For example, carbon nanorings (CNRs) with 20 nm outer diameters and 3.5 nm wall thickness, have shown outstanding performances as anode active materials: high lithium uptake and larger capacity, i.e. more than  $1200 \text{ mAh g}^{-1}$ , and over a hundreds of cycles at the current density of  $0.4 \text{ A g}^{-1}$ . Even at the higher current rates of  $45 \text{ A g}^{-1}$ , it has been observed a capacity as high as  $500 \text{ mAh g}^{-1}$ . The larger specific capacity and the high rate capability have been rationalized as due to the reduction of the diffusion distance and to the increase of the number of storage sites for Li-ions [81]. These advantages are paradigmatic results of the developing of nanosized carbon based materials.

### 2.1.1. Hard carbon

Even though soft carbons represent the state of art for anode materials in LIBs, some limitations, such as their low capacity and

the high voltage hysteresis during the delithiation process, might hinder their use as anode materials for the next generation of LIBs [12,82]. On the other hand, hard carbons have high reversible capacity (more than  $500 \text{ mAh g}^{-1}$ ) in the potential range  $0\text{--}1.5 \text{ V vs. Li/Li}^+$ , therefore they represent a valid alternative to soft carbons. Hard carbons were developed in 1991 by Kureha Corporation (Japan) and used as the negative electrode materials in the first built lithium-ion secondary battery, but they were subsequently dismissed from the electronic industry. Hard carbon have random alignment of graphene sheets which provides many voids to accommodate lithium, however the manner in which lithium diffusion occurs inside hard carbons makes lithium diffusion very slow, namely very poor rate capacity. Nevertheless, a number of automakers and battery companies have been focussing on the development of hard carbon for use in Electric Vehicles, mainly motivated by its high reversible capacity. Recently, anode capacity between  $200$  and  $600 \text{ mAh g}^{-1}$  has been reported [83–85]. This high capacity is associated to the material porous nature, number of graphene sheets and surface area [86]. However, hard carbons present two main drawbacks, namely low initial coulombic efficiency and low tap density. In order to overcome these problematics, a number of strategies has been pursuing, for example by means of surface oxidation, fluorination or by using metal coating or a thin layer of soft carbon [83,87]. In particular, the latter resulted in better lithium battery performance by improving both the coulombic efficiency and the lithium storage capacity. Further progress in this direction has been obtained through a systematic investigation of the effects of the temperature during the carbon coating process [87]. However, both the capacity and the cycling life of hard carbons still need to be improved. Haung et al. have synthesized porous structures of hard carbons and observed improved capacity, i.e. more than  $400 \text{ mAh g}^{-1}$  [88]. Interesting results have been observed with micron size hard carbon synthesized from potato starch. In fact, the results demonstrated reversible capacity of almost  $530 \text{ mAh g}^{-1}$  with good cycling life and rate capability [89]. Similarly, nano-porous hard carbons were synthesized from pyrolyzed sucrose and their electrochemical performances for LIBs were evaluated (see Fig. 3). These nanoporous materials exhibited remarkable capacity close to  $500 \text{ mAh g}^{-1}$  along with a good cycling life and rate capability. High rate capability has been demonstrated to be related to the fast lithium diffusion  $\sim 4.11 \times 10^{-5} \text{ cm}^2 \text{ s}^{-1}$  for hierarchical nanoporous hard carbon [84].

### 2.1.2. Carbon nanotubes

CNTs are characterized by highly ordered carbon nanostructures, realized through a self-assembly unidirectional growth process [37,90]. CNTs can be classified in single (SWCNTs) and multiwall carbon nanotubes (MWCNTs) depending on the thickness and on the number of coaxial layers. Since their discovery in 1991, both SWCNTs and MWCNTs were extensively investigated both as anode materials and as composites. In particular, when used together with other active anode materials, they exhibited better output than non CNT composite due to their superior electronic conductivity, good mechanical and thermal stability, adsorption and transport properties [37,90]. The maximum theoretical value obtained for the reversible capacity of CNTs has been estimated to be  $1116 \text{ mAh g}^{-1}$  for SWCNTs in  $\text{LiC}_2$  stoichiometry [91–94]. This is by far the highest capacity among carbon based active materials, and it has been attributed to the intercalation of lithium into stable sites located on the surface of pseudo graphitic layers and inside the central tube as well. However, to experimentally confirm the maximum theoretical predictions associated to CNTs/lithium is a major challenge. The research activity in CNTs as anodes is intense: several attempts were made with a variety of synthesis protocol and pre-treatments such as acid treatment and

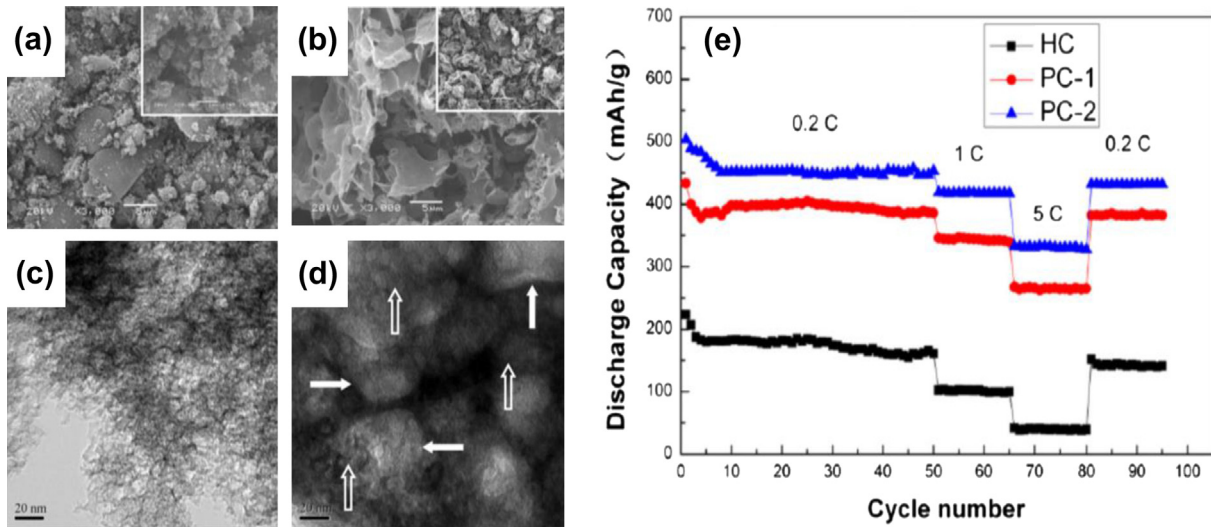


**Fig. 3.** SEM and TEM images of porous hard carbon-1 (a, c) and porous hard carbon-2 (b, d), respectively; (e) typical plot of their discharge capacities vs. number of cycles at various current rates. (From Ref. [84].)

ball milling surface modification [37,91]. Recently, Di Leo et al. reported that purified SWCNTs, produced by laser vaporization procedure, yield indeed the best lithium battery performance in terms of high capacity, i.e. more than  $1050 \text{ mAh g}^{-1}$  [95]. However, the achievement of high coulombic efficiency with CNTs remains challenging because of the presence of large structure defects and high voltage hysteresis. In order to overcome these issues, research has been focused on the morphological features of CNTs, such as wall thickness, tube diameter, porosity and shape (bamboo-like, quadrangular cross section, etc.) [96,97]. Particularly interesting is the approach that Oktaviano et al. have reported. In this work, chemically drilled MWCNTs have been synthesized by solid state reaction [98]. The process is summarized in Fig. 4. Cobalt oxide nanoparticles were wired onto the CNTs surface and an oxidation process was performed. Finally, the removal of oxide particles led to 4 nm size holes on the MWCNTs surface. The lithium battery performances of these structures were evaluated and they showed higher capacity, better cycling life and higher coulombic efficiency than pristine MWCNTs.

In order to improve the lithium storage capacity and the cycling life in batteries, CNTs conjugated with a variety of nanostructured materials (Si, Ge, Sn, Sn–Sb) or metal oxides ( $\text{M}_x\text{O}_y$ ;  $\text{M} = \text{Fe}, \text{Mn}, \text{Ni}, \text{Mo}, \text{Mo}, \text{Cu}, \text{Cr}$ ) have been synthesized [37,55,73,99–102]. These

hybrid systems result in CNTs with enhanced electrical conductivity and reduced volume changes during the charging and discharging processes. For example, Fan et al. reported that the uniform coating of  $\text{Fe}_3\text{O}_4$  onto aligned CNTs by magnetron sputtering leads to a capacity over  $800 \text{ mAh g}^{-1}$  with 100 charge–discharge cycles along with good rate capability [103]. Similarly, Mahanty's research group prepared  $\text{MoS}_2/\text{MWCNTs}$  composite. The electrochemical studies of this hybrid material showed a stable capacity of  $1030 \text{ mAh g}^{-1}$  at the 60th cycle [104].

Even though we have shown a number of interesting and promising results where CNT played a fundamental role, from the battery industry point of view the CNT technology is not yet considered mature enough. In fact, open issues regarding CNT mass production and cost presently hinder their use in LIBs applications.

### 2.1.3. Graphene

Graphene consists in a honey comb network of sp<sup>2</sup> carbons bonded into two dimensional sheets with nanometre thickness (single-atom thickness). Since the introduction of the term graphene in 1987, this material has drawn much attention because of its admirable properties and versatility in a number of fields such as chemical, physical, biological and engineering sciences [45,105]. Among its astonishing properties, we can recall good electrical

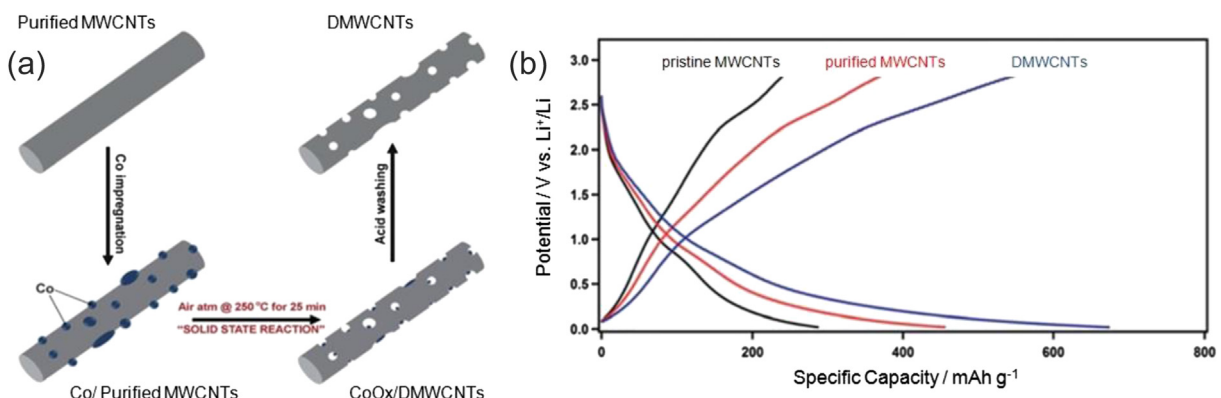


**Fig. 4.** (a) Schematic representation of the synthesis protocol for drilling multiwalled carbon nanotubes; (b) Charge–discharge profile of MWCNTs, purified MWCNTs and nano-drilled MWCNTs at the 20th cycle and current density  $25 \text{ mA g}^{-1}$ . (From Ref. [98].)

conductivity, relevant mechanical strength, high values of charge mobility and high surface area which make graphene a suitable electrode material for LIBs [45,73,106,107]. However, the theoretical lithium storage studies of graphene are quite controversial. In fact, even though the amount of lithium adsorbed by a single layer of graphene is low compared to graphite ( $372 \text{ mAh g}^{-1}$ ) [108], when a number of graphene sheets is considered together this value overtakes the graphite performance leading either to  $780 \text{ mAh g}^{-1}$  or to  $1116 \text{ mAh g}^{-1}$  [45,109,110]. These two values are associated to two different descriptions of the interaction between lithium and graphene. In particular, the former assumes absorption of Li-ions on both faces of graphene ( $\text{Li}_2\text{C}_6$  stoichiometry), while the latter assumes Li trapped at the benzene ring in a covalent bond ( $\text{Li}_2\text{C}_2$  stoichiometry).

Interestingly, the experimental research activity about graphene as anode material for LIBs is quite rich. Pan et al. prepared disordered graphene sheets by various methods: hydrazine reduction process, low-temperature pyrolysis and electron beam irradiation [110]. Electrochemical measurements demonstrated that graphene sheets exhibit high gravimetric capacity in the range  $790$ – $1050 \text{ mAh g}^{-1}$  due to the presence of additional active sites for lithium storage such as edges and other defects. However, the drawback of the disordered structure is the poor electronic conductivity. Similarly, to achieve high capacity from graphene anode in LIBs, Lian et al. proposed high quality graphite with few graphene layers ( $\sim 4$ ) and with a surface area over  $490 \text{ m}^2 \text{ g}^{-1}$ . Electrochemical studies have shown large reversible capacities close to  $1200 \text{ mAh g}^{-1}$  at the initial cycles, with values around  $848 \text{ mAh g}^{-1}$  even at the 40th cycle [111]. Recently, Wang et al. reported *in-situ* fabrication of doped hierarchically porous graphene (DHPG) electrodes for LIBs with ultrafast and long cycling capability [112]. As shown in Fig. 5, low and high magnification SEM and TEM images indicated that hollow graphene assemblies can contain small nanoscale pores. The electrochemical performance of DHPG electrodes exhibited high lithium storage with long cycling capability, around 3000 cycles, at a current density of  $5 \text{ A g}^{-1}$ . These promising results are attributed to the synergetic effects of the hierarchically porous structure, good conductive network and hetero-atom doping, which facilitate the mass transport and the speeding up the electrochemical reactions. Among the graphene class of materials, nanoribbons synthesized from MWCNTs hold promising potential in lithium storage capability. In particular, Fahlman's research group obtained both reduced and

oxidized graphene nanoribbons, the latter with increased lithium uptake and stable capacity of  $800 \text{ mAh g}^{-1}$  [113].

Presently, the LIBs research activity suggests, as suitable anode candidates, the use of various hybrid graphene/metals or semiconductors and graphene/metal oxides/phosphides [103,114–116]. For example, it is well known that  $\text{SnO}_2$  possess good anode properties, however its volume changes, while cycling, represents the major drawback for a good reversible capacity. This issue was faced by considering a graphene– $\text{SnO}_2$  particles composite. In fact, graphene can insert  $\text{SnO}_2$  nanoparticles, therefore supporting the electrical conductivity to  $\text{SnO}_2$ . In particular, it was recently proposed a hybrid system formed by  $2$ – $3 \text{ nm}$   $\text{SnO}_2$  particles/nitrogen doped graphene ( $1220 \text{ mAh g}^{-1}$  gravimetric capacity over 100 cycles) [117]. Similarly, silicon composite with carbon nanocables and reduced graphene oxide sheets showed excellent Li-ion battery performance by reaching a capacity value of  $1600 \text{ mAh g}^{-1}$  over 100 charge–discharge cycles along with high coulombic efficiency [118]. An alternative approach considered  $\text{Fe}_3\text{O}_4$  nanorods implanted onto graphene. This nanorod/graphene hybrid system showed a capacity retention of  $867 \text{ mAh g}^{-1}$  with only 5% loss from its initial capacity [119].

## 2.2. Titanium based oxides

Titanium based oxides have drawn significant attention in the lithium battery community because they allow the designing of operational devices with minor safety concerns. Moreover, this class of active materials shows other interesting features such as inexpensiveness, low toxicity, low volume change (2–3%) on both lithium insertion and de-insertion, along with an excellent cycling life [120–123]. However, it shows also low theoretical capacity, in the range  $175$ – $330 \text{ mAh g}^{-1}$ , and low electronic conductivity.

The electrochemical performance and the lithium insertion/removal capacity of titanium based oxides mainly depend on their structure, morphology and size. In particular, it has been found that nanostructured titanium oxides lead to better capacity, longer cycling life and higher rate capability than the bulk materials [60,123,124]. Hence, a lot of efforts have been spent in the development of anode materials based on nanostructured titanium oxides. To date, titanium dioxide with various allotropic forms and spinel  $\text{Li}_4\text{Ti}_5\text{O}_{12}$  have been extensively studied for anode purposes [120–122,125,126].

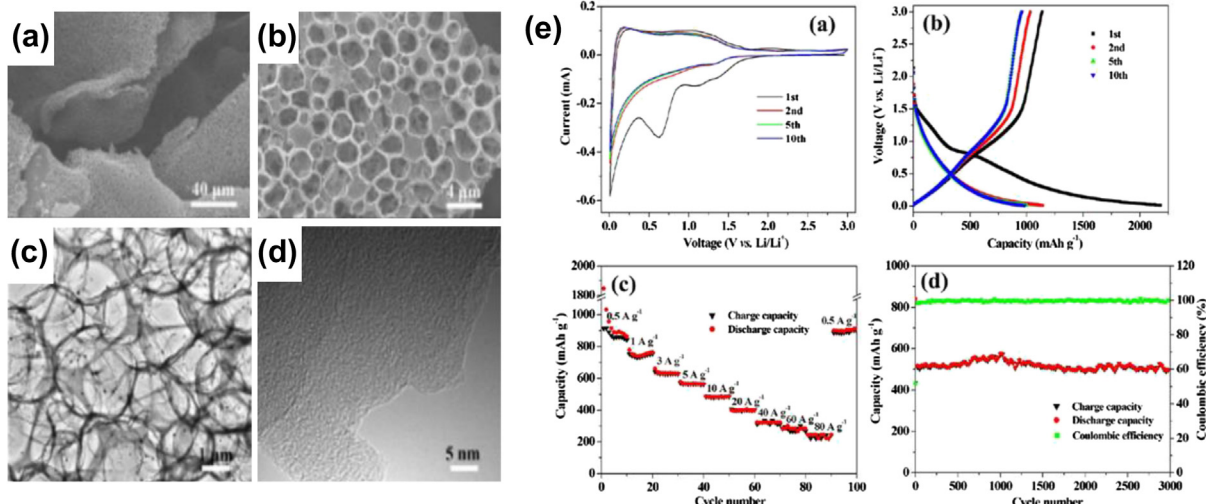


**Fig. 5.** (a, b) SEM, (c) TEM and (d) HRTEM images of doped hierarchically porous graphene (DHPG) electrodes; (e) Corresponding Electrochemical performance of DHPG electrodes. (From Ref. [112].)

### 2.2.1. Spinel $\text{Li}_4\text{Ti}_5\text{O}_{12}$ (LTO)

Spinel  $\text{Li}_4\text{Ti}_5\text{O}_{12}$  is considered the most appropriate titanium based oxide material for lithium storage purposes because it exhibits excellent Li-ion reversibility at the high operating potential of 1.55 V vs.  $\text{Li}/\text{Li}^+$ . Lithium insertion/extraction in LTO occurs by the lithiation of spinel  $\text{Li}_4\text{Ti}_5\text{O}_{12}$  yielding rock salt type  $\text{Li}_7\text{Ti}_5\text{O}_{12}$ . During the insertion process, the spinel symmetry and its structure remain almost unaltered [120,127,128]. The high operating potential guarantees safety conditions, in fact the formation of the solid electrolyte interface (SEI) is mitigated and the development of dendrites, typical issue in carbon based anodes, is avoided [129]. However, the low theoretical capacity of 175 mAh g<sup>-1</sup> and the low electronic conductivity  $\sim 10^{-13}$  S cm<sup>-1</sup> limit the full capacity at high charge–discharge rates and reduce the Li-ion diffusion [130]. To overcome these issues two approaches have been followed: the first one is to enhance the electronic conductivity of LTO by surface treatments [131,132], the second one consists in enhancing the Li-ion diffusion by downsizing the LTO to the nanoscale. Nanocrystalline LTO, with particle sizes between 20 and 50 nm, has been synthesized by simple combustion method in short time period (less than 1 min) [133]. An experimental discharge capacity, i.e. 170 mAh g<sup>-1</sup>, very close to the maximum theoretical value, was measured at 0.5C rate, while stable capacities of 140 and 70 mAh g<sup>-1</sup> were observed at higher charge–discharge rates of 10C and 100C, respectively. The doping of low conductivity materials, such as LTO, is one of the prominent techniques to enhance their electrical conductivity. In this regard, Shen et al. implemented a methodology for direct growing of LTO nanowires on titanium foil and they further showed an improvement in the conductivity of LTO nanowires by introducing  $\text{Ti}^{+3}$  ions through hydrogenation. The results were confirmed through XPS technique [134]. These nanowires containing Ti foil were directly used as electrodes without any conductive additives and binders, and they exhibited brilliant rate performance by reaching a capacity value close to the theoretical one, i.e. 173 mAh g<sup>-1</sup> at 0.2C rate with good cycle life. Moreover, this value became 121 mAh g<sup>-1</sup> at 30C (see Fig. 6). These nice results are related to the enhancement of the electron conductivity in hydrogenated LTO with respect to the pristine one. Furthermore, Xia's research group reported binary nanocomposites of  $\text{Li}_4\text{Ti}_5\text{O}_{12}$ – $\text{Li}_2\text{Ti}_3\text{O}_7$  for overcoming the LTO sudden voltage drop at the end of the charge–discharge process. These composites, having dimensions of few hundreds of nanometres, show a lamellar-like morphology formed by interconnected nanograins of  $\sim 20$  nm size. The composites exhibited superb electrochemical

performance, in terms of capacity and cycling life. Finally, their voltage profile could be altered by monitoring the composite ratio, therefore fulfilling the request of a smooth voltage output in order to prevent overcharging and over discharging [130].

### 2.2.2. Titanium dioxide ( $\text{TiO}_2$ , titania)

Titanium dioxide (titania) is a very promising material for anode applications in the LIBs field, in fact it is suitable for mass production and it is also cost effective. In addition, titania shows excellent safety and stability characteristics at the operative potential of 1.5 V vs.  $\text{Li}/\text{Li}^+$ . Moreover,  $\text{TiO}_2$  has admirable advantages such as high electro-activity, strong oxidation capability, good chemical stability, high abundance and structural diversity [120,121,135]. These features make titania a good candidate as anode material in LIBs, especially for HEV applications. Titania can host 1 mol of lithium per 1 mol of  $\text{TiO}_2$  with a theoretical maximum capacity of 330 mAh g<sup>-1</sup> and  $\text{LiTiO}_2$  stoichiometry (almost double than LTO). However, the exploitation of the entire capacity is a major experimental challenge. The lithium intercalation/de-intercalation process in titania typically depends on its crystallinity, particle size, structure and surface area [136–138]. Titania has several allotropic forms, the most well-known are rutile (tetragonal,  $\text{P}4_2/\text{mmn}$ ), anatase (tetragonal,  $\text{I}4_1/\text{amd}$ ) and brookite (orthorhombic,  $\text{Pbc}\alpha$ ) [139,140]. Even though anatase titania has been considered the most electroactive form, other allotropes such as rutile and brookites are also widely studied for anode purposes [136,141,142].

Regarding the rutile form of  $\text{TiO}_2$ , it has been shown that decreasing its particle size to 15 nm allows a larger capacity of 378 mAh g<sup>-1</sup> at first discharge and subsequent stable capacity of 200 mAh g<sup>-1</sup> (0.6 Li per one molecule of rutile  $\text{TiO}_2$ ) over 20 cycles, at the current density of 0.05 A g<sup>-1</sup>. With particle size of 300 nm, the initial and the 20th cycle capacities of 110 and 50 mAh g<sup>-1</sup> were observed, respectively [142]. The improvement of the capacity and the Li-ion uptake are related to the nanosize characteristic and to the high surface area. Similarly, it was reported that 6 nm particle size of  $\text{TiO}_2$  anatase maintains high capacity at more than 200 mAh g<sup>-1</sup> over 20 cycles at the current density of 0.1 A g<sup>-1</sup>. Furthermore, at the current rate of 10 A g<sup>-1</sup>, the capacity of 125 mAh g<sup>-1</sup> was attained. When moving to higher particle sizes of  $\text{TiO}_2$ , such as 15 nm and 30 nm, lower capacities of 80 and 71 mAh g<sup>-1</sup> were found, respectively [143]. In particular, the reduction in the particle size facilitates the lithium intercalation/de-intercalation and the electron collection at the anode by enhancing the Li-ions diffusion and shortening the charge path

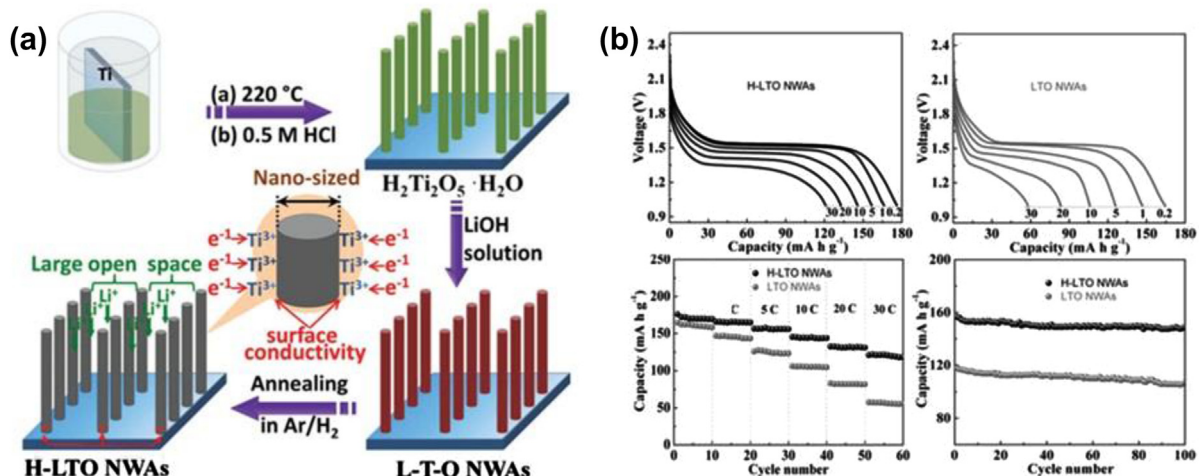


Fig. 6. (a) Schematic representation of the fabrication of hydrogenated-LTO (H-LTO); (b) Electrochemical performance of H-LTO and LTO nanowires. (From Ref. [134].)

length, respectively. In this regard, Lee's research group synthesized anatase  $\text{TiO}_2$  microspheres by solvothermal process. These  $\text{TiO}_2$  microspheres are formed by the combination of ultra-fine 6–8 nm  $\text{TiO}_2$  nanocrystals with 4–6 nm pore size microstructures. The optimal performances of  $\text{TiO}_2$  microspheres, such as high lithium storage capability, high number of charging–discharging cycles and high tap density were explained with their spherical morphology [123]. This last characteristic was in fact tuned to improve the capacity, the rate capability as well as the cycling life of titania based anodes [135,141]. For example, Gentili et al. synthesized, by means of hydrothermal route, nanotube of anatase  $\text{TiO}_2$  with wall thickness of 2–3 nm, an external diameter of 8–10 nm and length in the range 100–300 nm [144]. These nanotubes exhibited maximum capacity at around 300 mAh g<sup>-1</sup> with lithium uptake roughly 0.98 Li for unit formula of titania. Along with high capacity, these titania nanotubes showed high rate capability and good cycling life with a capacity around 250 mAh g<sup>-1</sup> over 100 charge–discharge cycles. Similarly, Brown et al. have synthesized mesoporous  $\text{TiO}_2$ –B microspheres, with 12 nm pore size [145]. This porous titania has proved to be a good anode material at different current densities. Interestingly, a lithium storage capacity of ~120 mAh g<sup>-1</sup> was attained at the high current rate of 60C. This improved rate performance was related to the fast kinetics from the pseudo-capacitive electrochemical behaviour of microspheres of  $\text{TiO}_2$ –B.

Further development of  $\text{TiO}_2$  in terms of power density and cycling life can be reached by combining titania nanostructures with conductive matrices such as carbon, CNTs and graphene

[146,147]. For example, as shown in Fig. 7, Wang et al. fabricated an hybrid composite of titania and graphene by hydrothermal procedure. The obtained structure consisted of 10 nm diameter  $\text{TiO}_2$  nanotube, with length from few hundreds to thousands of nanometres, built on a graphene layer [148]. The obtained specific capacity of this composite was more than 300 mAh g<sup>-1</sup> in the potential range from 1.0 to 3.0 V vs. Li/Li<sup>+</sup>. The stability of these hybrid composites was proved over few thousands of charge–discharge cycles, from low to high currents, namely from 10 mA g<sup>-1</sup>–8000 mA g<sup>-1</sup>, along with very good columbic efficiency. This promising results were possible due to the nanotube morphology and to the electronic interactions between the hybrid components.

### 3. Alloy/de-alloy materials

The next generation of LIBs is expected to fulfil the power demand of high energy consuming devices, to power electric vehicles and HEVs and to be used in stationary applications. Hence, the specific capacity is the fundamental parameter to be considered in novel anode active materials. Materials which can satisfy the requirement of high capacity are, for example, silicon, germanium, silicon monoxide and tin oxide which react with lithium according to an alloy/de-alloy mechanism. Their specific theoretical capacity ranges from 783 mAh g<sup>-1</sup> for tin oxide up to 4211 mAh g<sup>-1</sup> for silicon [149–151]. Even though these alloy based materials can provide larger specific capacity than graphite (372 mAh g<sup>-1</sup>) and

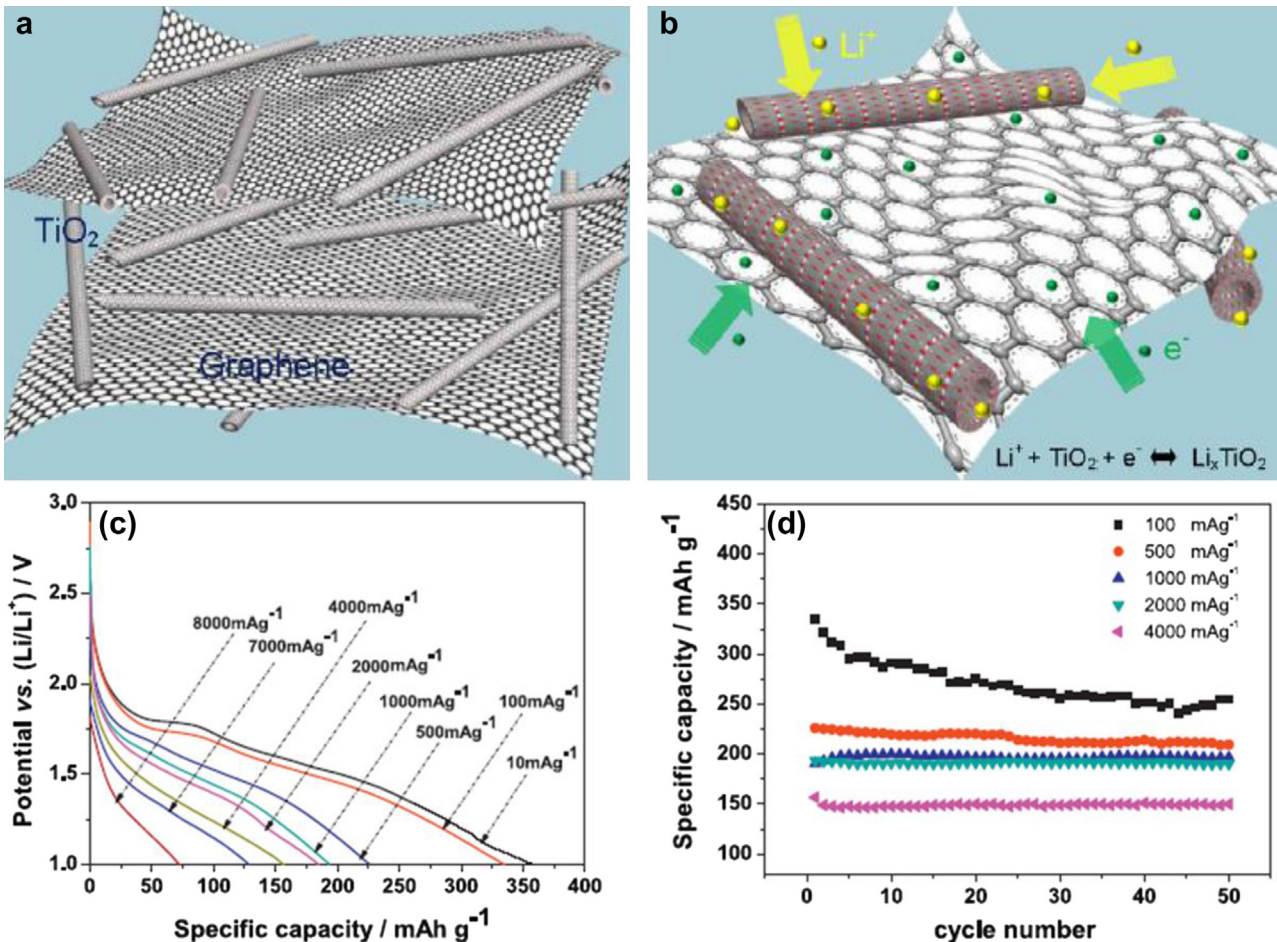


**Fig. 7.** Schematic illustration of (a)  $\text{TiO}_2$  nanotube/graphene (TG) composite; (b) electron transport through graphene and ion diffusion in the tubular  $\text{TiO}_2$ ; (c) Initial discharge capacities of TG composite electrodes at various current densities from 10 to 8000 mA g<sup>-1</sup>; (d) Cycling stability of TG composite at current densities from 100 to 4000 mA g<sup>-1</sup> (voltage range: 1.0–3.0 V). (From Ref. [148].)

LTO ( $175 \text{ mAh g}^{-1}$ ), the major drawbacks are the poor cycling life due to the high volume expansion/contraction and the larger irreversible capacity at the initial cycles. In order to overcome these issues, various approaches have been followed: the downsizing from micro to nanoscale particle and the fabrication of composites with both lithium active and inactive material, are the most promising. In the latter case the lithium active/inactive material serves as a conductive buffer matrix between the alloy materials and lithium source [152]. Nanostructured alloy materials with different morphologies like nanowires and nanotubes have been considered as an implementable path to achieve high capacity with a good rate capability and long cycling life [153,154].

### 3.1. Silicon (Si)

Silicon has both the highest gravimetric capacity ( $4200 \text{ mAh g}^{-1}$ ,  $\text{Li}_{22}\text{Si}_5$ ) and volumetric capacity ( $9786 \text{ mAh cm}^{-3}$ ) among the anode material candidates [155–159]. In addition, the discharge (lithiation) potential of silicon is almost close to graphite i.e.  $0.4 \text{ V vs. Li/Li}^+$ . Finally, Si is the 2nd most abundant element on earth, hence inexpensive and eco-friendly. It is then easily understood why silicon and its derivatives are considered the most promising and interesting materials for the realization of the future generation of LIBs, which justifies the strong academic and industrial interest for their development as anode active materials. The electrochemical lithiation of Si electrodes has been deeply investigated by many groups. It has been clarified that the high specific capacity value is due to the formation of intermetallic Li–Si binary compounds such as  $\text{Li}_{12}\text{Si}_7$ ,  $\text{Li}_7\text{Si}_3$ ,  $\text{Li}_{13}\text{Si}_4$ ,  $\text{Li}_{22}\text{Si}_5$  [156]. However, some issues prevent the employment of Si as anode in LIBs. Firstly, the large volume modification ( $\sim 400\%$ ) during the charge/discharge process causes poor cycling life and irreversible capacity. Secondly, the formation of Si compounds at the solid electrolyte interface inhibits the alloy/de-alloy process. In order to understand the exact reason of poor cycling stability of Si as anode in LIBs, many *in-situ* investigations with different experimental techniques such as XRD, NMR, TEM have been performed [160–164]. These studies evidenced that the electrical contact between the active material and both the conductive carbon and current collector undergoes a drop due to the large volume expansion/contraction of the Si anode, leading to an irreversibility of lithium insertion/extraction. Eventually, these volume changes result in shorter cycling life and capacity fading.

To overcome these issues, a lot of efforts were focused on nanostructured Si, especially on their morphology aspect. For example nanowires, nanotubes and nanospheres were considered due to their capability of providing the necessary free volume for accommodating the Si expansion during the alloying/de-alloying process. In particular, Si nanowires (Si NWs) and nanotubes have shown a reversible capacity over  $2000 \text{ mAh g}^{-1}$  with good cycling stability. The best results were obtained by the direct growth of Si NWs on the metallic current collectors, following a vapour–liquid–solid approach. Such technique gives better accommodation to the large volume changes and all the nanowires participate to the lithium alloy process because of the direct contact with the current collector [165]. This anode fabrication approach led to remarkable electrochemical performances. In fact, the observed charge–discharge capacity was  $3500 \text{ mAh g}^{-1}$  over 20 cycles at  $0.2\text{C}$  rate, while at the higher current rate of  $1\text{C}$  the capacity value was set at  $2100 \text{ mAh g}^{-1}$ . This impressive lithium storage results were possible due to the good electronic contact between the current collector and the Si NWs, to an efficient charge transport mechanism and to the small diameter of Si NWs, which allows better accommodation of the volume change without any initiation of fractures. Similarly, Yao et al. reported about composite nanofibers

formed by Si, lithium and highly electrical conductive materials such as TiC/C, fabricated by low pressure chemical vapour deposition [166]. These synthesized silicon composite nanofibers showed high specific capacity around  $2800 \text{ mAh g}^{-1}$  at  $0.2\text{C}$  current rate, with an excellent cycling life, over 100 charge–discharge cycles. When a higher  $2\text{C}$  current rate was considered, a specific capacity close to  $1500 \text{ mAh g}^{-1}$  was observed.

Despite the mentioned nanostructures showed superior electrochemical properties, their fabrication is not cost-effective, and thus this emerging technology is still not applicable at an industrial level. In order to move from an experimental proof-of-concept device towards the realization of effective anodes for LIBs, research groups are seeking for alternative fabrication methods such as the promising hydrothermal and solvothermal techniques. For example, Chan et al. introduced a new method to grow carbon coated Si NWs in solution. The main point was the carbon coating of Si NWs by means of their mixing with conductive matrices such as MWCNTs and with amorphous carbon [167]. The synthesized carbon coated Si NWs, showed stable reversible capacity of  $1500 \text{ mAh g}^{-1}$  and about 100 charge–discharge cycles at the current rate  $0.2\text{C}$ .

Similar approaches have been exploited to fabricate carbon coated Si NWs. An example is offered by the metal catalytic etching of silicon wafer in HF aqueous solution followed by carbon coating. The prepared carbon coated silicon nanowires exhibited reversible capacity around  $1326 \text{ mAh g}^{-1}$  [168]. Further improvements in the performances of Si NWs as anode were made by Ge et al. [48] with direct etching of boron-doped silicon wafers. The obtained porous Si NWs exhibited superior electrochemical performance and long cycling life. In fact, even after 250 cycles, the reported reversible capacities were  $2000$ ,  $1600$  and  $1100 \text{ mAh g}^{-1}$  at  $2$ ,  $4$  and  $8 \text{ A g}^{-1}$  current density, respectively. This impressive performance was possible due to the high porosity of silicon nanowires and to the improvement of the electronic conductivity through boron doping.

In other works, Si nanotubes demonstrated even larger reversible capacity up to  $2500 \text{ mAh g}^{-1}$  [156,169]. For example, Song et al. fabricated sealed tubular shape silicon nanostructures by chemical vapour deposition in a ZnO assisted approach [170]. These kinds of nanotubes are capable to accommodate the Si volume change during the lithiation/delithiation process, they show high initial coulombic efficiency together with discharging/charging capacities around  $3860$  and  $3360 \text{ mAh g}^{-1}$ , respectively. Interestingly, these high capacities are very close to the theoretical ones which indicates that all Si nanotubes are connected to the current collector and are fully reacting with lithium. In addition, electrochemical measurements evidenced stable capacities from  $2600$  to  $1490 \text{ mAh g}^{-1}$  at high current rate regimes from  $0.2\text{C}$  to  $2\text{C}$ . Similarly, carbon coated Si nanotubes were fabricated by Cho et al. with the use of alumina as template [171]. These carbon coated nanotubes showed the impressive capability to deliver large reversible charge capacity of  $3247 \text{ mAh g}^{-1}$  and high coulombic efficiency, close to 89%. In the perspective to introduce Si nanotubes as anodes into the commercial market, they have been tested by using standard cathode electrode, i.e.  $\text{LiCoO}_2$ . Li-ion technology, based on these materials, exhibited 10 times larger capacity than commercially available graphite based lithium cells, even after 200 cycles. This exceptional behaviour has been attributed to three main aspects: i) availability of free volume in the nanotubes for accommodating lithium, ii) amorphous phase dominance vs. the crystalline form during cycling, iii) carbon coating. Recently, Wu et al. developed stable Si double walled nanotubes surrounded by ion permeable silicon oxide shell as anode for advanced LIBs (as shown in Fig. 8) [172]. The thin layer of  $\text{SiO}_x$  on the Si nanotube allows the diffusion of Li-ions but, at the same time, it prevents direct contact with the electrolyte. These hybrid nanotubes showed outstanding stable anode performance with a cycling life over 6000

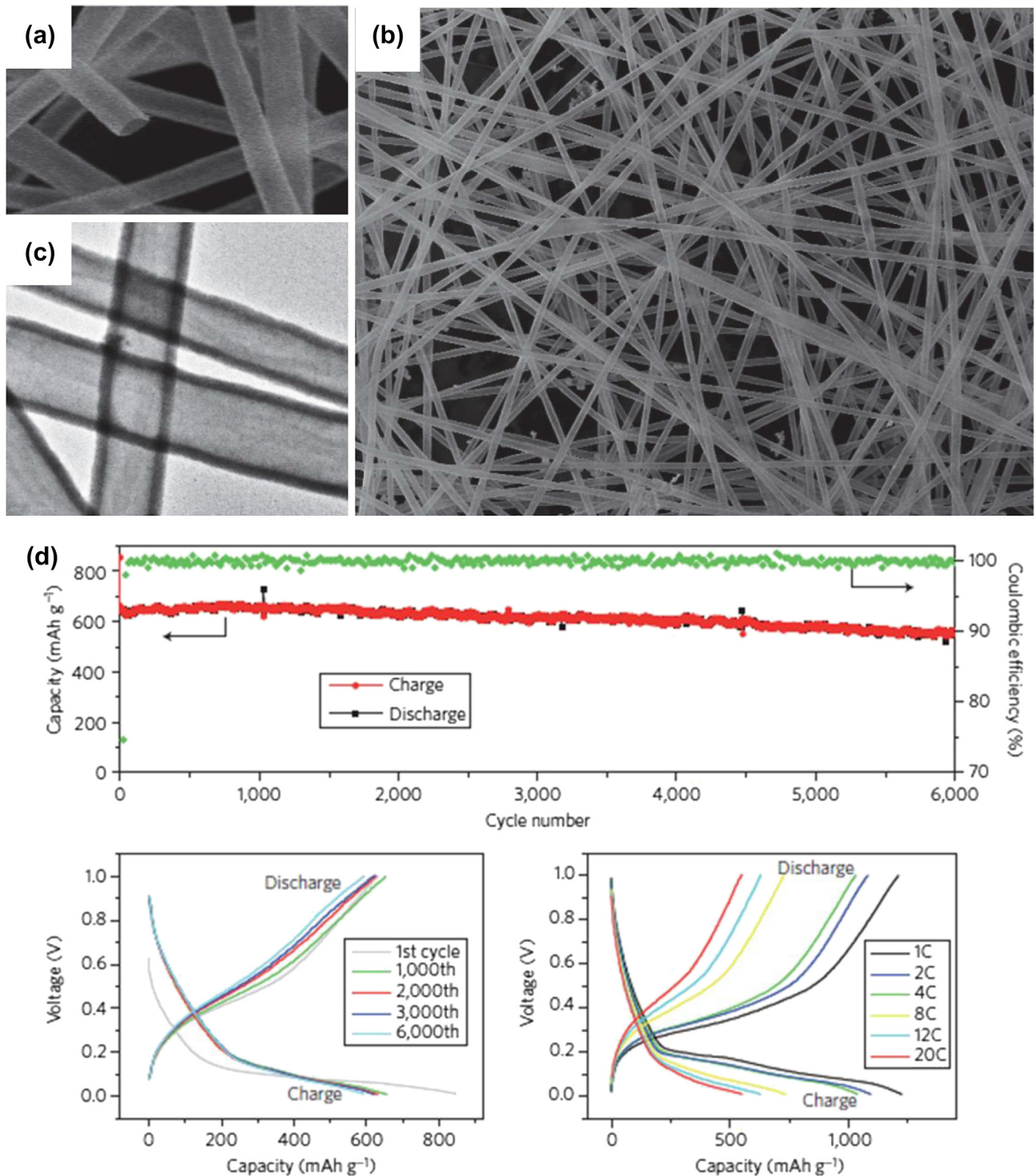


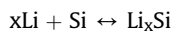
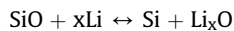
**Fig. 8.** (a, b) SEM and (c) TEM images of double-walled Si–SiO<sub>x</sub> nanotube (DWSiNTs); (d) Electrochemical charging–discharging cycling performance of DWSiNTs electrodes. (From Ref. [172].)

cycles, with a specific capacity retention close to 88% and with a superior coulombic efficiency.

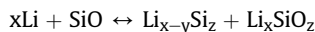
### 3.2. Silicon monoxide ( $\text{SiO}$ )

$\text{SiO}$  is considered an alternative choice to silicon, as anode candidate, due to its high theoretical capacity ( $>1600 \text{ mAh g}^{-1}$ ). In

addition, lithium oxygen co-ordination implies minimal volume change and, at the same time, lower activation energy [173–176]. The electrochemical reactions happening during the charge–discharge process determine the conversion of  $\text{SiO}$  into  $\text{Si}$  and lithium oxides and, possibly, the formation of  $\text{Si–Li}$  or, alternatively, the direct formation of  $\text{Si–Li}$  alloy and lithium silicates. The mechanism can be schematized as follows:



(or)



Solid SiO is thermodynamically unstable at all temperatures. Therefore, it can be transformed into Si and SiO<sub>2</sub> in a temperature triggered disproportionation reaction [177,178]. As previously pointed out about silicon, also SiO undergoes consistent changes in the volume during the lithiation and de-lithiation processes. Moreover, both the electrical conductivity and the lithium insertion/de-insertion rates remain quite poor [179,180]. To solve these problems and to improve the reversible capacity as well as the cycle retention, different approaches have been tested. The most promising are carbon coating, electrochemical reduction of SiO with lithium and, finally, the size reduction of SiO [181,182]. Among these solutions, particle size reduction combined with carbon coating is an effective way to overcome the above issues by shortening the diffusion distance of Li-ions and thus to enhance the ionic and the electrical conductivities.

In 2002 it was demonstrated the effect of both the oxygen concentration and particle size on the cycling life and on the reversible capacity of SiO<sub>x</sub> [47]. The lithium battery analysis performance was carried out by changing the oxygen concentration of SiO, such as SiO<sub>0.8</sub>, SiO and SiO<sub>1.1</sub>, along with the particle size, such as 30 and 50 nm. It was observed that SiO<sub>0.8</sub> with 50 nm particle size shows the high capacity of 1700 mAh g<sup>-1</sup> at initial cycles accompanied by large capacity fading over cycling. However, when SiO<sub>1.1</sub> was considered, a stable capacity over cycling of 750 mAh g<sup>-1</sup> was found. The conclusion was that lower oxygen contents in SiO<sub>x</sub> allow for higher specific capacity associated to poorer cycling life. In addition, also the particle size was found to affect the anode performance. In particular, 30 nm SiO<sub>x</sub> particle size showed better capacity retention with high reversible capacity compared to larger particles.

Finally, it is interesting to notice that in order to understand the electrochemical reaction mechanisms between SiO and lithium, various analytical techniques have been employed, such as X-ray, photoelectron spectroscopy, NMR, high resolution TEM and electrochemical dilatometry [183–188]. In particular, <sup>29</sup>Si Magic Angle Spinning (MAS) NMR, <sup>7</sup>Li MAS NMR and HRTEM experiments were carried out at various discharge/charge potentials of SiO electrode with lithium. From these results it has been suggested that Si–Li alloy, along with LiO<sub>x</sub> and Li–Si–O ternary, were the intermediate products of reversible electrochemical reactions [187]. Hence, further investigations on SiO electrode for LIBs are still required.

Recently Liu et al. [173,189] published an interesting work about SiO composites containing highly conductive intermetallic compounds, such as Sn–Co–C and Sn–Fe–C, which have the advantages of good cycleability and high tap density. However, they also present the major drawback of low reversible capacity which make their performance not better than graphite. Hence, the authors realized a composite by combining these intermetallic materials with an anode showing high theoretical capacity, such as SiO. This led to new kinds of hybrid materials which are expected to overcome the volume expansion problem of SiO and to achieve high capacity with good cycling stability. Therein, tin acts as active phase with lithium while the transition metal (i.e. Cobalt or Iron) serves as a tin alloying buffer layer, inactive to lithium. These composites exhibited stable capacity of 700–900 mAh g<sup>-1</sup> over a large number of charge–discharge cycles.

Further achievements regarding SiO anodes have been reached with the synthesis of three-dimensional porous SiO. The realization

of 3-D porous structures of SiO has been accomplished by depositing silver nanoparticles on SiO, followed by chemical etching in hydrofluoric acid solution. The best performances in terms of lithium reversibility and cycleability were observed with the carbon coating of the 3-D porous SiO, where the carbon source was acetylene gas [190]. Carbon coated 3-D porous SiO represents an effective way to achieve improved electrochemical conductivity and low volume expansion during the cycling process. In fact, carbon coated porous SiO have shown an excellent capacity around 1490 mAh g<sup>-1</sup> over 50 charge–discharge cycles at 0.1C. A good response was also observed at the larger current rates of 3C and 5C with stable capacities of 1100 and 920 mAh g<sup>-1</sup>, respectively [190]. Recently, structurally and kinetically stable hierarchical SiO<sub>x</sub> ( $0.9 < x < 1$ ) nanoconifers were reported by Song's group for applications as anode material in LIBs [174]. Columnar-shape SiO<sub>x</sub> nanoconifers were directly self-assembled on metallic NiSi<sub>x</sub> nanowires by means of chemical vapour deposition technique (see Fig. 9). These SiO<sub>x</sub> nanoconifers revealed stable charge–discharge performance over a hundred of charge–discharge cycles with specific capacity close to the theoretical one, along with good coulombic efficiency and high rate capability compared to bulk SiO<sub>x</sub>. This exciting result is due to the high conductivity of the metallic NiSi<sub>x</sub> core, which assists the efficient charge transport pathway from/to SiO<sub>x</sub> phase.

### 3.3. Germanium (Ge)

Germanium is an extensively studied active anode material owing to its high lithium storage capability (1623 mAh g<sup>-1</sup>) with Li<sub>22</sub>Ge<sub>5</sub> as equivalent stoichiometry and reversible alloy/de-alloy reactions [150,191]. Even though Ge is considerably more expensive and shows lower capacity than silicon, it has desirable advantages such as high intrinsic electrical conductivity (10<sup>4</sup> times higher than silicon), higher capacity than graphite anode and a narrow band gap (0.67 eV). Furthermore, it has been reported that the lithium diffusion into Ge is 15 and 400 times faster than in Si at 360 °C and at room temperature, respectively. This ensures higher rate capability and more efficient charge transport than in silicon and graphite as well [150,192]. Ge high power capability is then extremely important in advanced high power density applications such as electric vehicles. However, as discussed for silicon, the practical usage of Ge as active electrode in LIBs is hindered by the dramatic volume change (~300%) during lithium insertion/de-insertion [150,193]. Ge nanostructures, such as nanoparticles [194], nanowires [192] and nanotubes [171,195] can effectively sustain the volume change with better efficiency than bulk and microstructures. Noticeably, improvements have been observed with hybrid composite of Ge nanoparticles using conductive matrices, obtained through simple preparation routes, for example solid state pyrolysis [196].

For example, Ge nanoparticles, with diameter between 5 nm and 20 nm, were encapsulated inside carbon nanospheres with diameters in the range from 50 to 70 nm [196]. The role of the carbon nanospheres is to act as structural buffer and electro-active material during the lithium insertion and de-insertion process and to avoid direct contact with the electrolyte. This last aspect prevents Ge from the formation of SEI. These obtained composites exhibited highly reversible lithium storage along with high rate capability.

Similar behaviour has been observed in Ge nanoparticles deposited on SWCNTs by CVD [197]. Crystalline Ge nanoparticles, with an average size of 60 nm, were deposited on SWCNTs and coated with a thin layer of titanium for better rate capability. The major advantage of using CNTs is the increase of the conductivity between Ge and the current collector together with the increase

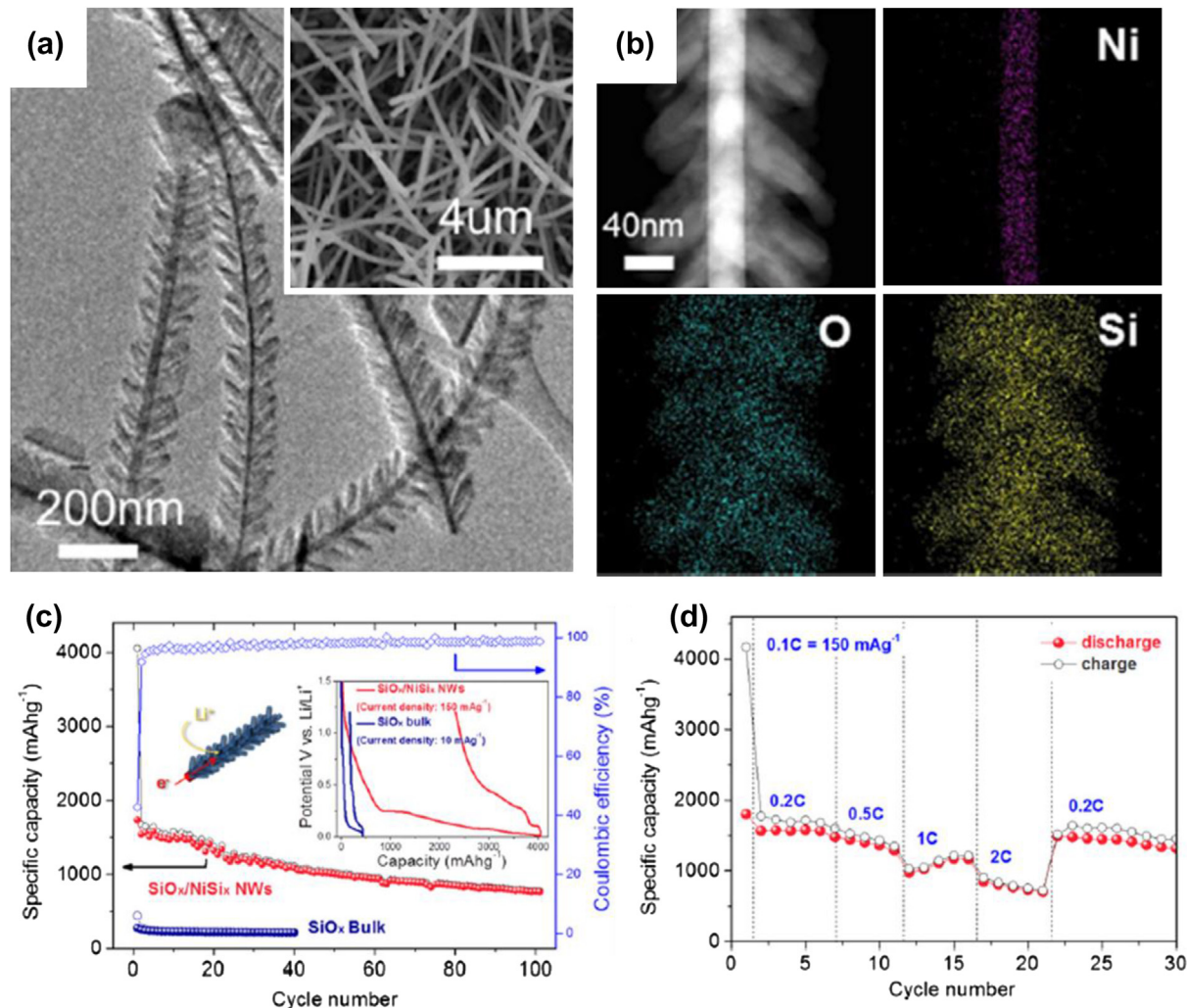


**Fig. 9.** (a) TEM image of SiO<sub>x</sub> nanoconifer on NiSi<sub>x</sub> nanowires (NWs) (inset: SEM image of SiO<sub>x</sub>/NiSi<sub>x</sub> NW); (b) scanning TEM-HAADF images and EDX elemental colour map of single SiO<sub>x</sub>/NiSi<sub>x</sub> NW; (c) electrochemical cycling stability along with coulombic efficiency and specific capacity vs. charge/discharge cycle numbers of SiO<sub>x</sub>/NiSi<sub>x</sub> NWs (inset: galvanostatic charge–discharge curves in the range of 0.01 and 1.2 V); (d) cycling performance of SiO<sub>x</sub>/NiSi<sub>x</sub> NWs at different current rates. (From Ref. [174].) (For interpretation of the references to colour in this figure legend, the reader is referred to the web version of this article.)

of the lithium diffusion which, in turn, means accommodation of Ge volume expansion while cycling. This hybrid Ge nano composite showed excellent anode capacity around 980 mAh g<sup>-1</sup> vs. lithium metal and 800 mAh g<sup>-1</sup> with LiFePO<sub>4</sub> as cathode. Similarly, comparable high reversible capacities, along with excellent cycling life and high rate capability, were achieved by combining Ge nanoparticles with MWCNTs and reduced graphene oxide [49,198].

Nanostructured germanium nanowires and nanotubes have been investigated as well. For example, Yuan et al. proposed alkanethiol-passivated Ge NWs as anode in LIB [199]. Firstly, Ge NWs were synthesized through gold-seeded growth process. Secondly, HF solution was used to attain H-terminated Ge NWs which, in turn, underwent surface passivation of thiol by using dodecanethiol. The electrochemical performances of thiol-passivated Ge NWs showed remarkable results such as high reversible specific capacity of 1130 mAh g<sup>-1</sup> along with a good cycling life at 0.1C. These structures were also proved to possess high power capability with a reversible capacity of 550 mAh g<sup>-1</sup> at the higher current rate of 11C. For a better understanding of the passivation effect of Ge NWs in LIBs, comparison experiments with Ge nanoparticles and unpassivated Ge NWs were also carried out. Both electrochemical

and microscopy techniques confirmed that the surface passivation of Ge NWs leads to better structure integrity.

Similarly, hybrid metal/Ge nanostructures have also been fabricated and tested. For example, Wang et al. synthesized three dimensional Cu–Ge core–shell nanowires by direct RF-sputtering of Ge layer on previously prepared Cu nanowires [200]. These nanowires delivered large reversible capacity of 1419 mAh g<sup>-1</sup> even after 40 cycles. They also attained a brilliant rate capability with capacities of 850 and 734 mAh g<sup>-1</sup> at the current rates of 40C and 60C, respectively. These exciting results can be rationalized by considering that Cu nanowires act as good electrical contact between substrate and Ge, thereby facilitating electron transfer and charge collection by shortening the lithium diffusion length.

Finally, nanoscale germanium oxides were also studied as novel anode material for LIBs. Very recently, Seng et al. improved germanium dioxide (GeO<sub>2</sub>) electrochemical performance by using Ge with a conductive carbon coating [201]. GeO<sub>2</sub>/Ge/C was prepared in a three steps process, starting with the synthesis of GeO<sub>2</sub> from hydrolysis of GeCl<sub>4</sub> and followed by carbon coating with acetylene gas, resulting in GeO<sub>2</sub>/C. The last step was the reduction of GeO<sub>2</sub>/C to GeO<sub>2</sub>/Ge/C through high temperature ~650 °C. The

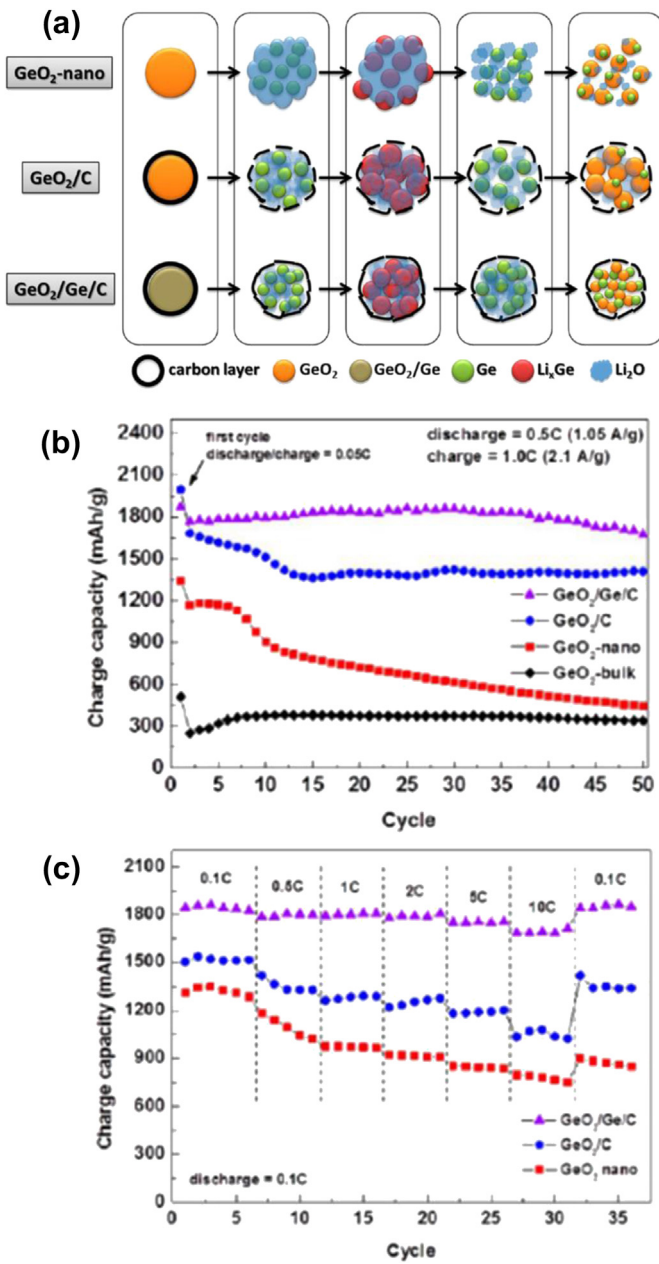


**Fig. 10.** (a) Schematic representation of the lithium reaction mechanism in Ge,  $\text{GeO}_2\text{-C}$  and  $\text{GeO}_2\text{/Ge/C}$ ; (b) Cycling performance of all samples for 50 cycles at 1C rate; (c) performance of all samples from 0.1 to 10C. (From Ref. [201].)

analysis of the lithium battery performance was carried out for materials such as  $\text{GeO}_2\text{/Ge/C}$ ,  $\text{GeO}_2\text{/C}$ , nano  $\text{GeO}_2$  and bulk  $\text{GeO}_2$ . The  $\text{GeO}_2\text{/Ge/C}$  composite showed high capacities of 1860 and 1680 mAh g<sup>-1</sup>, with good cycling stability, at the current rates of 1C and 10C, respectively (see Fig. 10). Such a notable Li battery performance was related to the carbon coating of Ge, in particular it was found that carbon enhances the reversibility of the conversion reaction of  $\text{GeO}_2$  with lithium.

#### 3.4. Tin oxide ( $\text{SnO}_2$ )

Tin oxide was firstly developed by Fuji Photo film corporation and it received significant attention as anode in Li-ion batteries due to the high theoretical capacity and low work potential, i.e. 0.6 V vs. Li/Li<sup>+</sup> [12,51,52,127]. The electrochemical lithium alloying reactions

can be summarized in a first partially irreversible step, where  $\text{SnO}_2$  is reduced into Sn and lithium oxides ( $\text{SnO}_2 + 4\text{Li} \leftrightarrow \text{Sn} + 2\text{Li}_2\text{O}$ ), which is followed by the reversible Sn–lithium alloying/de-alloying reaction ( $\text{Sn} + 4.4\text{Li}^+ \leftrightarrow \text{Li}_{4.4}\text{Sn}$ ). This overall electrochemical process involves 8.4Li for one  $\text{SnO}_2$  formula unit. The corresponding theoretical capacity is 1491 mAh g<sup>-1</sup> but it is reduced to 783 mAh g<sup>-1</sup> when the second highly reversible step is reached. Hence, 783 mAh g<sup>-1</sup> is commonly considered as the actual theoretical capacity. Furthermore, severe electrode degradation is observed because of the consistent volume change (>200%) upon cycling. Therefore, a lot of attention has been paid to improve the cycling stability of  $\text{SnO}_2$  and to reduce the irreversible capacity caused by volume change [51,127].

Porous nanostructures, nanocomposites, and hollow nanostructured  $\text{SnO}_2$  have been proposed to overcome the above specified issues [51,202,203]. In particular, it was shown that porosity in nanostructured  $\text{SnO}_2$  is capable of balancing the volume changes during the lithium insertion/de-insertion. In fact, the pores act as buffer for the large volume changes. In this regard, Yin et al. prepared  $\text{SnO}_2$  mesoporous spheres in the range 100–300 nm from tin sulphate, by cost-effective and easy solution method [204]. The prepared  $\text{SnO}_2$  spheres showed notable lithium battery performance with capacities of 761 and 480 mAh g<sup>-1</sup> after 50 charge–discharge cycles at current densities of 200 mA g<sup>-1</sup> and 2000 mA g<sup>-1</sup>, respectively. Similar results were observed with mesoporous  $\text{SnO}_2$  using silica as template and, when compared to  $\text{SnO}_2$  nanowires, it was found the former providing better electrochemical response than the latter. In particular, the mesoporous  $\text{SnO}_2$  exhibited a reversible capacity of 800 mAh g<sup>-1</sup>, with capacity retention of 98%, even after 50 cycles at 0.2C current rate [202]. Responsible of this improved performance is the porosity of  $\text{SnO}_2$ , which allows the flooding of the electrolyte among the particles together with the buffering role for volume changes during the charge–discharge cycles.

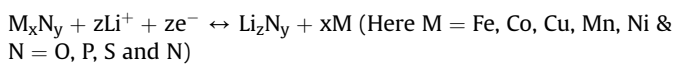
Due to the significant importance of carbon in the lithium batteries field, further developments were obtained by using composite carbon based materials such as carbon coated  $\text{SnO}_2$ ,  $\text{SnO}_2$ /nanofibers,  $\text{SnO}_2$ /carbon nanoparticles,  $\text{SnO}_2$ /CNTs and  $\text{SnO}_2$ /graphene [203,205–207]. In this regard, carbon free and carbon coated  $\text{SnO}_2$  hollow microspheres, prepared through cost-effective hydrothermal route where glucose was used as carbon source, were proposed [203]. The results showed better performance for the carbon-coated  $\text{SnO}_2$ , in terms of storage capacity, columbic efficiency and cycling life. This achievement was explained in terms of electrochemical oxidation of Sn, leading to  $\text{SnO}$  in carbon coated  $\text{SnO}_2$ . In fact, the electrochemical oxidation of Sn was not observed in carbon free  $\text{SnO}_2$ . Similarly, Jiang et al. proposed the use of graphene, as support for porous  $\text{SnO}_2$ , to enhance the lithium storage capacity and the cycling life. This hybrid composite was prepared by using electrostatic spray deposition technique and it was found to possess very good characteristics for lithium battery purposes [208]. The proper assembly of  $\text{SnO}_2$  on graphene is considered highly beneficial for lithium battery performance because it enhances the electrical conductivity and, at the same time, it can provide mechanical support of the active nanoparticles (i.e.  $\text{SnO}_2$ ) during charging and discharging process. The electrochemical outcome of this hybrid system were large stable capacities of 551 and 507 mAh g<sup>-1</sup>, up to the 100th cycle, at current densities of 200 and 800 mA g<sup>-1</sup>, respectively. Similar results were observed with hierarchical carbon encapsulated in tin embedded in graphene nanosheet composites. The synthesis protocol of this hybrid composite undergoes three main steps: i) assembly of  $\text{SnO}_2$  on graphene, ii) reduction of  $\text{SnO}_2$  into Sn nanoparticles, iii) carbon coating of the composite via CVD procedure. The final structure was directly used as anode in LIBs [209].

In addition to these examples, various morphological structures of  $\text{SnO}_2$  have been widely investigated such as nanowires, nanotubes, nanorod, nanoboxes and nanosheets, just to name a few [210–215]. For example, Ye et al. reported the effect of the size of  $\text{SnO}_2$  nanotubes on the anode performance [211]. Different lengths of  $\text{SnO}_2$  were synthesized through an hydrothermal process by using pre-fabricated mesostructured silica nanorods as sacrificial

template. Short size  $\text{SnO}_2$  nanotubes showed better electrochemical behaviour in terms of capacity and cycling life. The measured discharge capacity was  $468 \text{ mAh g}^{-1}$  after 30 cycles (see Fig. 11). This prominent outcome is thought to be related to the hollow characteristic of the nanotubes, that alleviate the volume changes and the mechanical stress during the cycling process.

#### 4. Conversion materials

In this section we will provide an overview on the transition metal compounds such as oxides, phosphides, sulphides and nitrides ( $M_xNy$ ;  $M = \text{Fe}, \text{Co}, \text{Cu}, \text{Mn}, \text{Ni}$  and  $N = \text{O}, \text{P}, \text{S}$  and  $\text{N}$ ) when utilized as anodes in LIBs. The electrochemical reaction mechanism involving these compounds together with lithium, implies the reduction (oxidation) of the transition metal along with the composition (decomposition) of lithium compounds ( $\text{Li}_xNy$ ; here  $N = \text{O}, \text{P}, \text{S}$  and  $\text{N}$ ). Anodes based on these compounds exhibit high reversible capacities ( $500\text{--}1000 \text{ mAh g}^{-1}$ ) owing to the participation of a high number of electrons in the conversion reactions [56,127,216]. The electrochemical conversions reactions can be described as follows:



##### 4.1. Iron oxide

Iron based oxides have been extensively studied for rechargeable lithium batteries because of their low cost, non-toxicity and high natural abundance. Iron oxides, both haematite ( $\alpha\text{-Fe}_2\text{O}_3$ ) and magnetite ( $\text{Fe}_3\text{O}_4$ ), are capable of participating in reversible conversion reactions with lithium, providing a theoretical capacity of  $1007$  and  $926 \text{ mAh g}^{-1}$ , respectively [217]. However, iron oxides tend to exhibit poor cycling performance due to low electrical conductivity, low diffusion of Li-ions, high volume expansion and iron aggregation during charging and discharging. Therefore, to overcome the above identified limits, many recent investigations have been focused on developing new methods for the preparation of iron oxide nanomaterials as well as for modifying their size, shape and porosity [218–222]. Other studies have been focused on methods to stabilize their structure and to improve the electrochemical kinetics and power capability, mainly by carbon coating or by carbon based composites of  $\alpha\text{-Fe}_2\text{O}_3$  and  $\text{Fe}_3\text{O}_4$  [223–225].

For example, Wang et al. reported  $\alpha\text{-Fe}_2\text{O}_3$  hollow spheres as anode in LIBs [226]. Hollow spheres of  $\alpha\text{-Fe}_2\text{O}_3$  have been synthesized by a facile quiesiemulsion template method. In particular, water and glycerol were used for this purpose, in fact their mixing leads to the formation of quiesiemulsion droplets, which served as soft template for the formation of  $\alpha\text{-Fe}_2\text{O}_3$  hollow spheres. The electrochemical reaction of  $\alpha\text{-Fe}_2\text{O}_3$  hollow spheres with lithium was studied in the potential window of  $0.005\text{--}3 \text{ V vs. Li/Li}^+$ . The results revealed high lithium reversibility accompanied by a storage capacity higher than  $700 \text{ mAh g}^{-1}$  for about one hundred of charge-discharge cycles. These investigations on  $\alpha\text{-Fe}_2\text{O}_3$  hollow spheres suggested that the morphology of the nanosized  $\text{Fe}_2\text{O}_3$  plays a significant role in the reactivity with lithium. Similarly, Wu et al. have studied the size and morphology effect of  $\alpha\text{-Fe}_2\text{O}_3$  nanorods in the range from  $300$  to  $500 \text{ nm}$  length with and without porosity [227]. Liu et al. prepared haematite  $\alpha\text{-Fe}_2\text{O}_3$  nanotubes with outer diameter ranging from  $200$  to  $300 \text{ nm}$  by using  $\text{ZnO}$  as sacrificial template. Next, they proceeded with carbon coating using glucose as carbon source [219]. The prepared  $\alpha\text{-Fe}_2\text{O}_3$  nanotubes showed good lithium insertion and de-insertion reversibility with a capacity close to  $750 \text{ mAh g}^{-1}$  over  $150$  charge-discharge

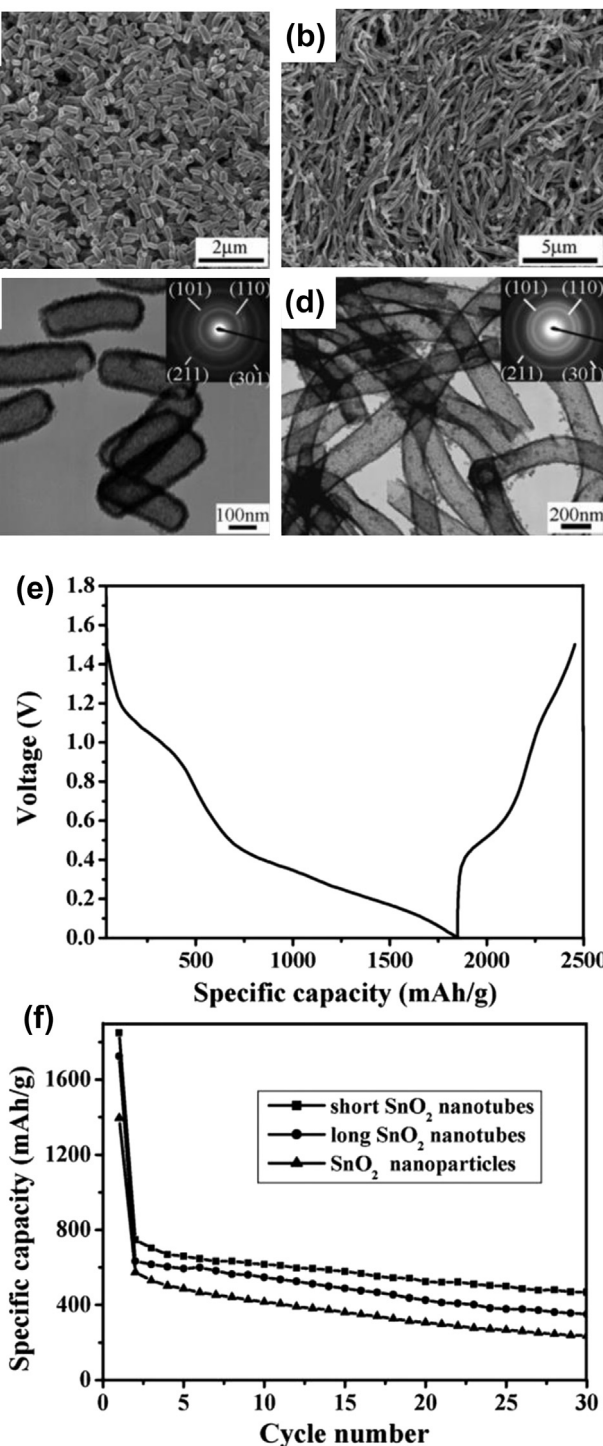


**Fig. 11.** (a, b) SEM and (c, d) TEM images of short and long  $\text{SnO}_2$  nanotubes, respectively; (e) plot of the first charge/discharge cycle of short  $\text{SnO}_2$  nanotube electrodes; (f) Cycling performance of various  $\text{SnO}_2$  samples at a current density of  $100 \text{ mA g}^{-1}$ . (From Ref. [211].)

cycles. The set current rate was 0.2C in the potential range 0.005–3 V vs. Li/Li<sup>+</sup> [219]. Similarly, carbon-decorated crystalline Fe<sub>3</sub>O<sub>4</sub> nanowires were synthesized by Murali et al. through microwave-assisted hydrothermal approach, using PEG-400 as soft template and polysaccharide as carbon source [228]. The resulted carbon decorated Fe<sub>3</sub>O<sub>4</sub> nanowires, with diameter ranging from 20 nm to 50 nm and length of several micrometres, showed excellent electrochemical stability with a good reversible capacity of 830 mAh g<sup>-1</sup> without any capacity damage over 50 cycles. These results are attributed to the positive role played by carbon in realizing a fast and highly reversible conversion reaction of iron oxides with lithium, which provides good electronic conductivity, enhanced lithium permeability and electrochemical stability. Recently, Xu et al. prepared spindle-like porous  $\alpha$ -Fe<sub>2</sub>O<sub>3</sub> from an iron-based metal organic structure, formed by nanoparticles with dimensions around 20 nm [229]. These novel  $\alpha$ -Fe<sub>2</sub>O<sub>3</sub> structures showed great enhancement of lithium storage with a reversible capacity of 911 mAh g<sup>-1</sup> at 0.2C current rate for more than 50 charge–discharge cycles. In addition, the capacity of 424 mAh g<sup>-1</sup> was achieved at the higher current rate of 10C. These promising results indicate that both size and morphology strongly affect both rate and lithium storage capability of iron oxides.

Sohn et al., through an aerosol-assisted process, followed by vapour coating, synthesized nanocomposites of Fe<sub>3</sub>O<sub>4</sub> cores and porous carbon–silicate layers. Carbon was chosen for its characteristic of increasing the electrical conductivity, hence to mitigate the aggregation of iron oxides particles and to reduce the mechanical stress during cycling [230]. These nanocomposites showed quite stable capacity around 900 mAh g<sup>-1</sup> with a coulombic efficiency close to 100% over 50 charge–discharge cycles. Very recently, nanoparticulate Fe<sub>2</sub>O<sub>3</sub> tubes have been obtained from microporous organic nanotubes (MONT) used as template [220]. The prepared porous Fe<sub>2</sub>O<sub>3</sub> nanotubes (FNT, see Fig. 12) exhibited excellent electrochemical performances with large capacities such as 918 and 882 mAh g<sup>-1</sup> at current densities of 500 and 1000 mA g<sup>-1</sup>, respectively. These results indicate that low cost iron based oxides with highly conductive carbon composites can be a valid alternative to graphite anodes.

#### 4.2. Cobalt oxides

In this section we will consider the recent advances on the research related to cobalt oxides materials (Co<sub>3</sub>O<sub>4</sub> and CoO) used as anode for LIBs. Co<sub>3</sub>O<sub>4</sub> and CoO show theoretical capacities of 890 and 715 mAh g<sup>-1</sup>, respectively [231,232]. Similarly to other kinds of materials, a number of different forms of cobalt oxides have been studied. Porous nanostructures, nanosheets, nanocubes, nanowires and nanotubes have been prepared by various synthetic routes such as wet chemical, solid-state, hydrothermal and microwave, therefore allowing the tailoring of their electrochemical performance [233–237]. For example, Guan et al. developed a template free method for the preparation of pure phase CoO octahedral nanocages by simply utilizing NH<sub>3</sub> as a co-ordination etching agent [238]. Therein, uniform size of the octahedral nanocages, with edge length of 100–200 nm, were obtained. In the test as anode material, they exhibited excellent cycling performance along with a good rate capability and enhanced lithium storage capacity, as seen in Fig. 13. Even at the high current rate of 5C, these octahedral nanocages were able to deliver a reversible capacity of 474 mAh g<sup>-1</sup>. Their large capacity and the high rate capability were possible owing to the existing huge voids which can accommodate the large volume changes. Recently, Wang et al. reported mesocrystal Co<sub>3</sub>O<sub>4</sub>nanoplate synthesized by solid state crystal reconstruction from Co(OH)<sub>2</sub> nanosheets [225]. The obtained porous Co<sub>3</sub>O<sub>4</sub>nanoplates showed

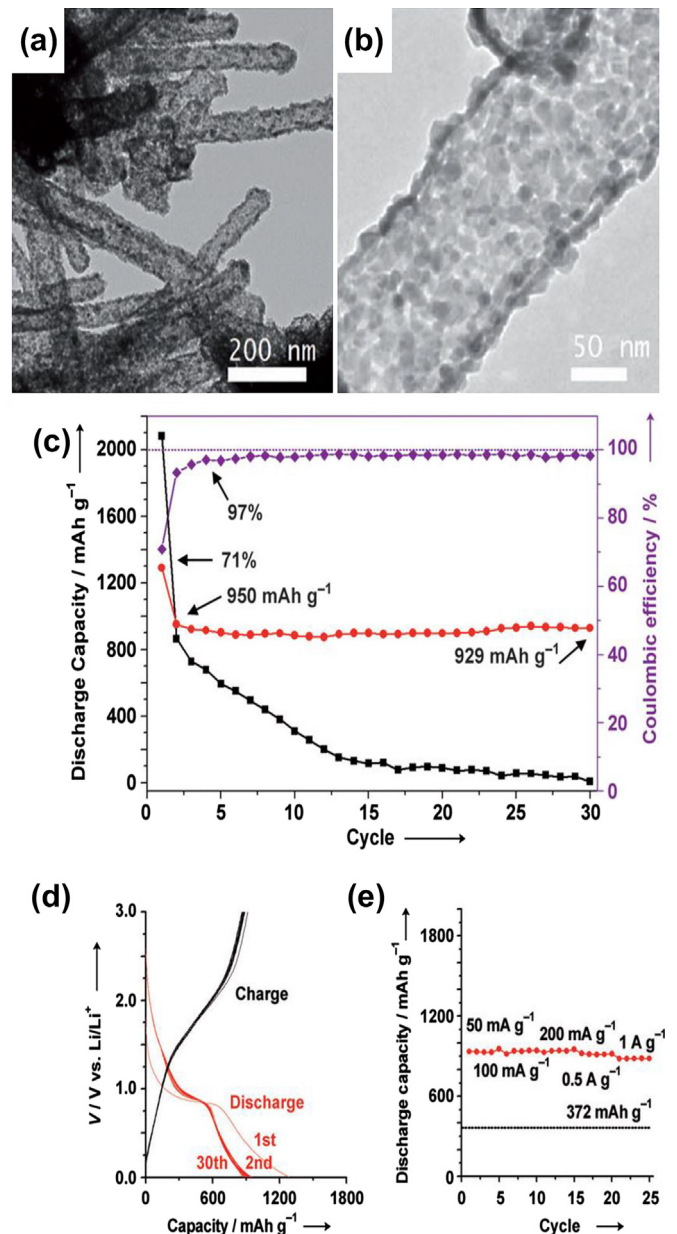


**Fig. 12.** (a, b) TEM images of Fe<sub>2</sub>O<sub>3</sub> nanotubes (FNTs) from MONT template; Li-ion battery performance of FNTs, (c) discharge capacity vs. number of cycles of FNTs (red) and commercial Fe<sub>2</sub>O<sub>3</sub> nanoparticles (black). The coulombic efficiency of FNT is also included (violet); (d) galvanostatic charge–discharge curves; (e) cycling performance of FNT at different current rates. (From Ref. [220].) (For interpretation of the references to colour in this figure legend, the reader is referred to the web version of this article.)

superior electrochemical performance with low initial irreversible capacity along with stable cycling performance. Discharge capacity of 1015 mAh g<sup>-1</sup> was observed even after 30 cycles at the current rate of 0.2C. This amazing output was attributed to the 2-dimensional nature of the nanoplates together with their porosity that facilitates the accommodation of volume expansion during the charge/discharge process.

Further composites of cobalt oxides have been studied to buffer the volume changes and to prevent the detachment and the agglomeration of cobalt oxides during the lithium insertion/extraction process. As previously described, especially carbon based composites are intensively studied due to their desirable properties. For example, ultra-fine CoO nanoparticles with size ~5 nm, densely anchored on graphene nanosheets, were fabricated by

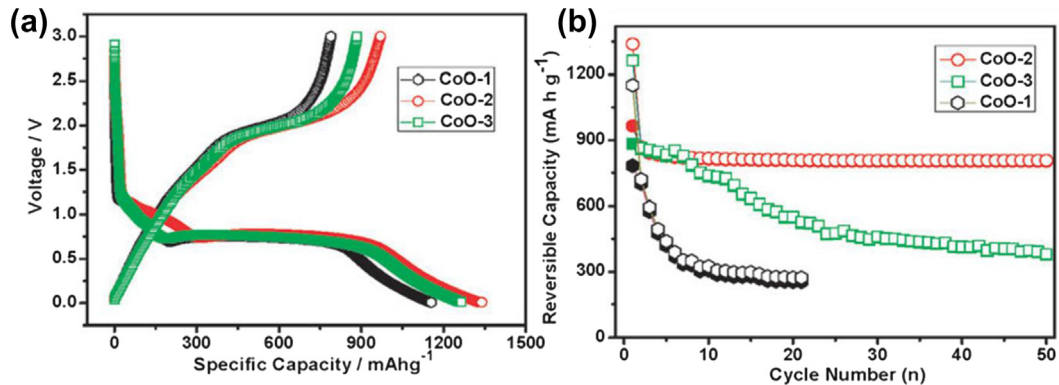


Fig. 13. (a) Galvanostatic first charge–discharge curves and (b) cycling performance for three CoO samples at the current rate of 0.2C. (From Ref. [238].)

Haung et al. [239]. The resulted CoO/graphene composites exhibited excellent lithium storage for a long charge–discharge cycling with 100% coulombic efficiency. Stable capacity of 1015 mAh g<sup>-1</sup> was maintained for 520 charge–discharge cycles. In fact, transmission electron microscopy analysis showed that the original morphology of CoO nanocomposites was preserved during such amount of cycles. This impressive result indicates that composites of CoO, with an electrically conductive network, can lead to high structural stability and enable long cycling life. A different morphology was introduced by Peng et al. who reported about

quantum dots of CoO/graphene composites and their high lithium storage capacity [240]. Similarly, Wu et al. prepared 10–20 nm Co<sub>3</sub>O<sub>4</sub> particles size anchored on graphene nanosheets in basic aqueous solution starting from Co<sup>+2</sup> inorganic salt and graphene [241]. This Co<sub>3</sub>O<sub>4</sub>/graphene nanocomposites displayed superior electrochemical performance with high reversible capacity, good cycling life and good rate capability.

Various other metal oxides, showing a conversion reaction mechanism with lithium, have also been studied. For example NiO, MnO<sub>x</sub>, CuO<sub>x</sub>, MoO<sub>x</sub>, CrO<sub>x</sub> were extensively investigated as anode

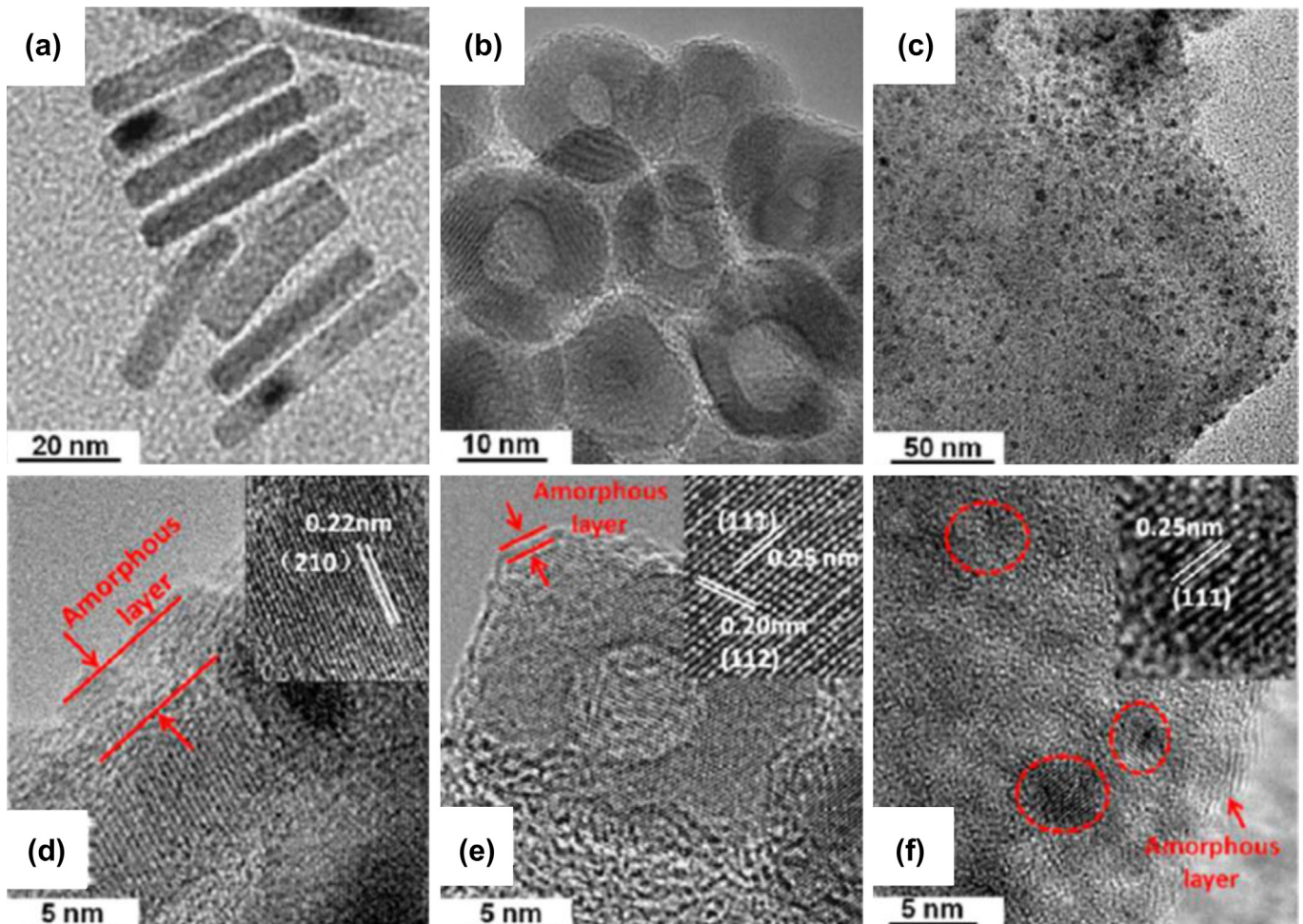
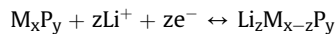


Fig. 14. TEM and HRTEM images of Co<sub>x</sub>P nanostructures, (a, d) Co<sub>2</sub>P rods; (b, e) CoP hollow spheres; (c, f) fine CoP nanoparticles. (From Ref. [259].)

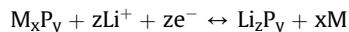
materials for LIBs and they showed miscellaneous physico-chemical properties and a large reversible capacity around  $500 \text{ mAh g}^{-1}$  [242–249].

#### 4.3. Metal phosphides ( $\text{MP}_x$ )

Metal phosphides have also been deeply studied as anodes for rechargeable lithium batteries [55,58,250–255]. They can react with lithium, both in a conversion reaction schema and in an intercalation/de-intercalation reaction, depending on the nature of the transition metal and on phosphorous bonding stability upon electrochemical environment. It is possible to divide  $\text{MP}_x$  into two groups. The first one involves the lithium insertion/extraction without breaking the metal–phosphorous bond, known as insertion/de-insertion mechanism:



The second group involves a conversion reaction mechanism. In such electrochemical reactions the bonds between metal and phosphorous are broken, resulting in nanosized metal particles and Li-phosphides:



Copper, cobalt, iron, nickel and tin based phosphides are usually considered to belong to the second group, i.e. conversion mechanism. Nevertheless, some reports showed that  $\text{MP}_x$  could

participate to the insertion as well as the conversion mechanism with respective to potential vs.  $\text{Li}/\text{Li}^+$  [59,256]. Metal phosphides can deliver high capacities between 500 and  $1800 \text{ mAh g}^{-1}$ . In addition,  $\text{MP}_x$  as anode, show an high degree of electrons delocalization, which leads to low formal oxidation state and strong covalent bond of M–Phosphorous. Another advantage is the lower insertion potential of  $\text{MP}_x$  than their oxide counterparts. However,  $\text{MP}_x$  usually have low electrical conductivity and high volume changes upon charge–discharge cycling. The use of  $\text{MP}_x$  as anodes deserves further exploration to overcome these drawbacks. For example, cubic  $\text{Ni}_2\text{P}$  crystals and lithiated  $\text{NiP}_2$ , were prepared through the milling of a mixture of nickel powder and red phosphorus. Furthermore,  $\text{Li}-\text{Ni}-\text{P}$  ternary active composites were also synthesized. Both  $\text{Ni}_2\text{P}$  and  $\text{Li}-\text{Ni}-\text{P}$  showed reversible lithium reactions in electrochemical environment. Especially the ternary composites exhibited a high reversible capacity of  $600 \text{ mAh g}^{-1}$  by conversion process [257]. Another approach was followed by Lu et al., who prepared carbon decorated hierarchical nanostructures of  $\text{NiP}_2$  spheres with an uniform size of 5–10 nm. The synthesis was based on an organic-phase mixture of nickel acetylacetone, trioctylphosphine, tri-n-octylamine, and oleylamine, together with oleyamine as surfactant [258]. By introducing the carbon decoration into  $\text{Ni}_2\text{P}$ , it was possible to enhance the capacity retention of lithium and to improve the structural stability by suppressing the aggregation and the pulverization of  $\text{Ni}_2\text{P}$  particles. The electrochemical performance of these small size  $\text{Ni}_2\text{P}$  spheres resulted in a capacity of  $365 \text{ mAh g}^{-1}$  at the current rate of 0.5C with a good reversible lithium charge–

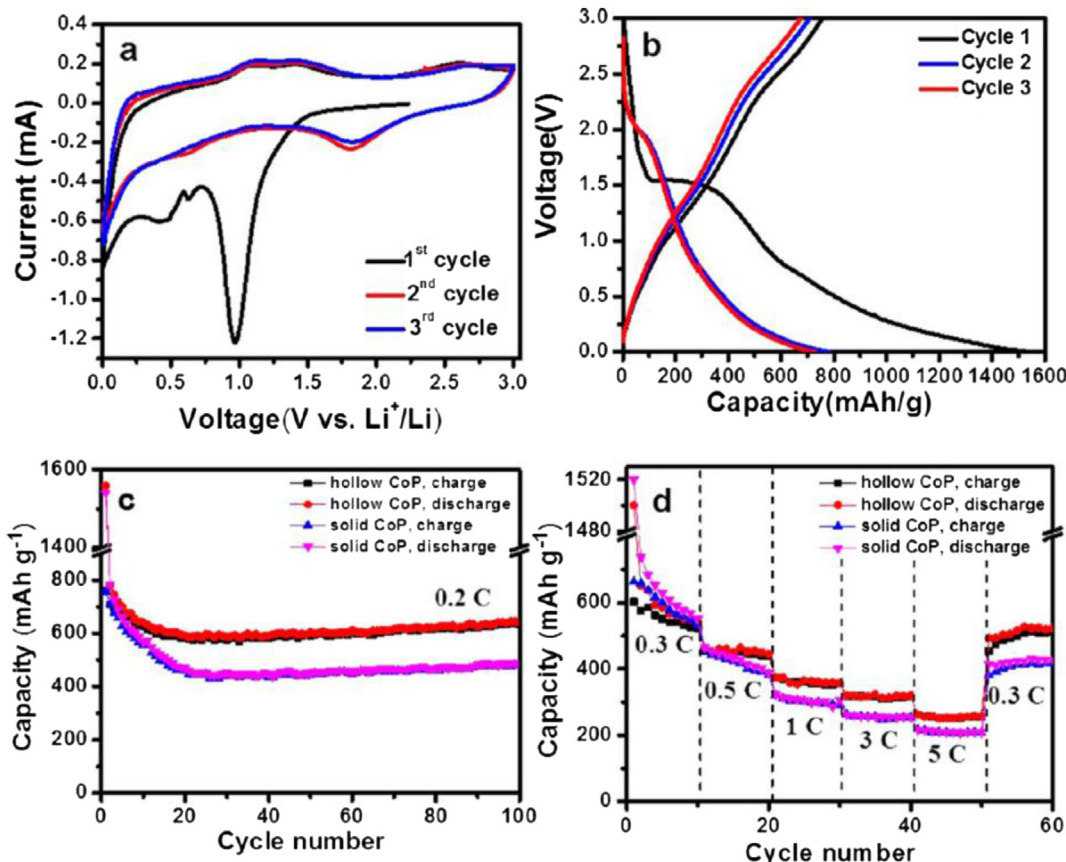


**Fig. 15.** (a) Cyclic voltammograms of the first three cycles of CoP hollow particles in the potential range of 0.005–3.0 V vs.  $\text{Li}/\text{Li}^+$  at the scan rate of  $0.5 \text{ mV s}^{-1}$ ; (b) galvanostatic charge/discharge profiles for hollow CoP nanoparticles at the current density of  $0.2\text{C}$ ; (c, d) comparison of cycling performances of CoP hollow and solid particles at  $0.2\text{C}$  and at different current rates. (From Ref. [259].)

discharge capability. In order to improve the lithium storage capacity with high cycling stability, the same research group synthesized carbon composites of mono phase  $\text{Ni}_5\text{P}_4$  by solution chemistry. In fact, an increase of the phosphorus concentration within nickel lead to a high theoretical capacity while the carbon coating was introduced to generally enhance the lithium battery performance [256]. The carbon shell on the surface of  $\text{Ni}_5\text{P}_4$  was achieved by thermal calcination at high temperatures. The galvanostatic charge–discharge measurements of  $\text{Ni}_5\text{P}_4/\text{C}$  as anode showed a specific capacity of  $644 \text{ mAh g}^{-1}$  after 50 cycles at the current rate 0.1C. Even at the higher current rate of 3C, it has been shown a noticeable capacity of  $357 \text{ mAh g}^{-1}$ . This interesting improvement is due to the high crystallinity of  $\text{Ni}_5\text{P}_4$  combined with the amorphous carbon shell.

Similar lithium performance was reported with copper and cobalt phosphides as well. Yang et al. prepared  $\text{Co}_x\text{P}$  particles with carbon layer coating of various morphologies such as nanorods, spheres, and hollow structures in solution phase with oleylamine (see Figs. 14 and 15) [259]. In particular, the electrochemical investigations of  $\text{CoP}$  hollow nanoparticles, coated with a carbon layer, showed higher capacity retention together with stable cycling and good rate capability than  $\text{Co}_2\text{P}$  nanorods and spheres. Their hollow peculiarity allows indeed an efficient lithium conversion reaction and, at the same time, it accommodates the volume changes during the charge–discharge process, thus leading to enhanced specific capacities and stability. Similarly, Trizio et al., reported size controlled hexagonal-like morphology of  $\text{Cu}_3\text{P}$  nanostructures for LIBs [260]. Furthermore, Villevieille et al. prepared  $\text{Cu}_3\text{P}$  nanorods from vaporized phosphorus and copper nanorods. This novel active electrode, i.e. the nanostructured  $\text{Cu}_3\text{P}$ , was also tested for LIBs applications [251].

#### 4.4. Metal sulphides ( $\text{MS}_x$ ) and nitrides ( $\text{MN}_x$ )

Other kinds of materials, which have been thoroughly investigated for anode applications in the LIBs field, are the transition metal sulphides ( $\text{MS}_x$ ) and nitrides ( $\text{MN}_x$ ). Iron, molybdenum, tin, antimony, nickel, cobalt and tungsten have attracted major interest due to their high lithium storage capability and structural advantages during the lithium insertion/de-insertion process [56,127,261–265]. As anticipated in the previous sections,  $\text{MS}_x$  and  $\text{MN}_x$  reaction mechanisms with lithium involve the reduction to metal and, respectively, the formation of lithium–sulphur and lithium–nitride, through conversion reaction. For instance, Wang et al. reported phase controlled polyhedron  $\text{CoS}_x$  prepared by solid state reaction. The synthesis procedure was based on a high temperature Co–sulphur powders reaction in presence of potassium halide (KX). Therein, KX served as reaction agent [266]. In particular,  $\text{CoS}_2$  and  $\text{CoS}$  were the most promising composites exhibiting superior reversible lithium insertion and extraction reaction, hence resulting in capacities of  $929$  and  $835 \text{ mAh g}^{-1}$ , respectively. In another approach, Paoletta et al. prepared nanoplates of  $\text{Fe}_3\text{S}_4$  using sulphur and thiosulfate, octadecylamine, iron salt and 3-methyl catechol [263]. Therein, 3-methyl catechol acted as phase control agent and growth moderator as well. Furthermore, cyclic voltammograms of  $\text{Fe}_3\text{S}_4$  electrode showed good reversible lithiation/delithiation process [267]. Similarly, composites of conductive matrices of carbon and graphene were also reported. For example, ultra-thin carbon coated  $\text{FeS}$  ( $\text{C}@{\text{FeS}}$ ) nanosheets were prepared by surfactant assisted solution method [268]. Here the carbon coating served to avoid the dissolving of lithium sulphides ( $\text{Li}_x\text{S}$ ), intermediate product of the metal sulphide formation during cycling, into the organic electrolyte inside LIBs. Owing to this advantage

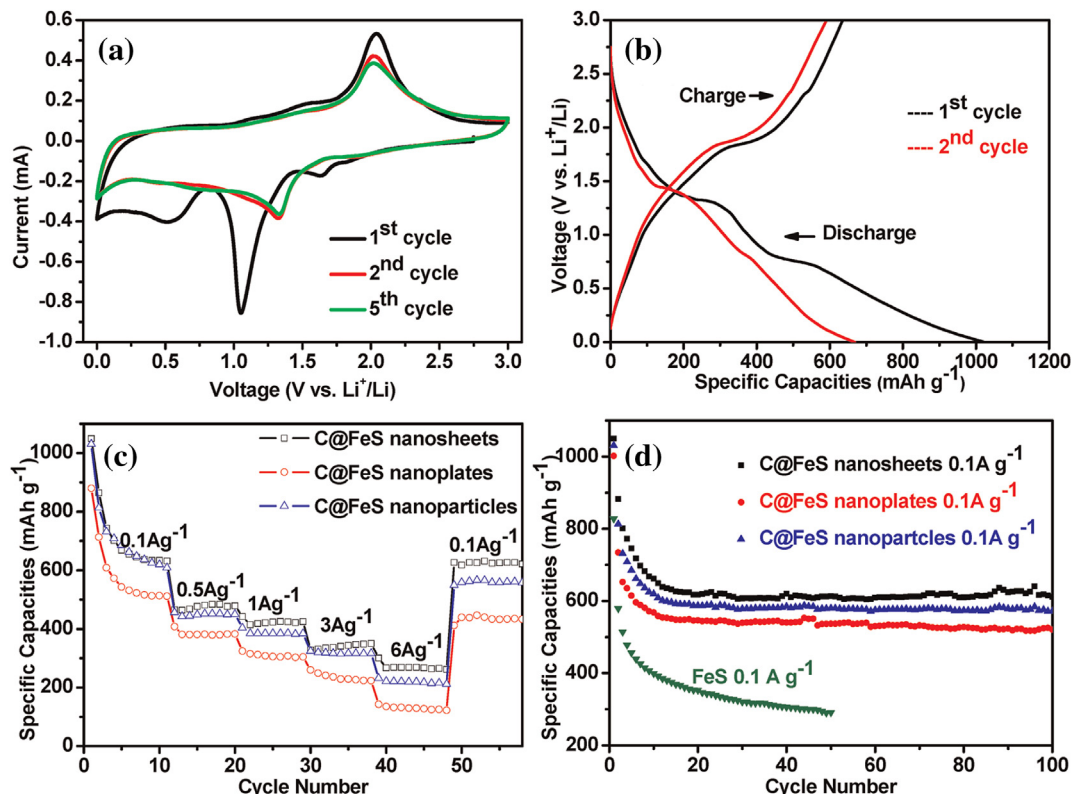


**Fig. 16.** (a) Cyclic voltammograms of the  $\text{C}@{\text{FeS}}$  nanosheets electrode from potential window between  $0$  and  $3 \text{ V}$  vs.  $\text{Li}/\text{Li}^+$  at the scan rate of  $0.5 \text{ mV s}^{-1}$ ; (b) galvanostatic charge–discharge voltage curves of  $\text{C}@{\text{FeS}}$  nanosheets electrode at the current density of  $0.1 \text{ A g}^{-1}$  for the 1st and 2nd cycles; (c, d) cycling performance of  $\text{C}@{\text{FeS}}$  nanosheets, nanoplates and nanoparticles at various current densities. (From Ref. [268].)

provided by the carbon coating, 2-dimensional C@FeS nanostructures exhibited very interesting LIBs performance (see Fig. 16), with stable 100 cycles capacity of  $615 \text{ mAh g}^{-1}$  at the current rate of 0.16C and voltage between 0.01 and 3.0 V vs. Li/Li<sup>+</sup>. Interestingly, even at the current rate of 10C, it resulted in a reversible capacity of  $235 \text{ mAh g}^{-1}$ . A similar electrochemical behaviour was also observed for graphene wrapped CoS nanoparticles [269]. These impressive results indicate that metal sulphides can represent a valid alternative as materials anode in future LIBs.

Besides metal sulphides, also metal nitrides have emerged as promising anodes for LIBs. Among them, Cu<sub>3</sub>N, VN, Co<sub>3</sub>N, CrN, Fe<sub>3</sub>N, Mn<sub>4</sub>N and Ni<sub>3</sub>N have especially been studied [56,127,270–273]. Gillot et al. prepared Ni<sub>3</sub>N by various synthetic routes, such as ammonolysis of nickel salts, or nickel particles, and thermal decomposition of nickelamide in the presence of ammonia [274]. In particular, Ni<sub>3</sub>N from nickelamide showed the best electrochemical performances, with the largest capacity ( $1200 \text{ mAh g}^{-1}$ ). Moreover, Ni<sub>3</sub>N exhibited also a good rate capability, with a reversible capacity of  $500 \text{ mAh g}^{-1}$  sustained in 10cycles at the current rate of 1Li per hour (see Fig. 17). Similarly, large discharge capacity ( $1200 \text{ mAh g}^{-1}$ ) was achieved with Cr<sub>3</sub>N thin films by Sun et al. [275]. Nanopowder of Cu<sub>3</sub>N has been reported in a conversion reactions with Li<sub>3</sub>N and Cu particles, and the obtained first cycle discharge capacity was  $675 \text{ mAh g}^{-1}$  [272]. Das et al. prepared nanoflakes of CoN films by RF magnetron sputtering [273]. The galvanostatic charge–discharge measurements with lithium metal in the range 0.005–3 V vs. Li/Li<sup>+</sup> showed an initial capacity close to  $760 \text{ mAh g}^{-1}$ , however it was also observed a huge irreversibility in the first cycle due to SEI formation. Interestingly, upon cycling, the capacity increased consistently up to  $960 \text{ mAh g}^{-1}$ , value observed after 80 cycles. From this result was deduced that the CoN electrode takes a certain number of cycles to reach a stable configuration.

Along with the above specified anode nanostructures, an important research field involves the use of conversion-alloy based materials, having the characteristic of undergoing reversible conversion reaction followed by reversible alloy reaction with lithium. It has been reported that lithium can form alloys with several metals such as Al, Si, Sn, Sb, In, Zn, Pb, Bi, Ag, Pt, Au, Cd, As, Ga and Ge [61,150,276–279]. However, few of them, together with their corresponding compounds such as intermetallic, oxide or phosphide, were studied in the anode perspective for lithium batteries [51,56,278]. These anodes can react with lithium, first through conversion, then through alloy reactions at a potential that depends on the selected material. In particular, metal oxides like SiO, SnO, GeO<sub>x</sub> have already been discussed in the present review. Intermetallic compounds based on Sn, Sb, Bi, Si, such as Zn<sub>x</sub>Sb, SnSb, InSb, MnSb, Ag<sub>x</sub>Sb, and AlSb, have been extensively studied [142,278–282]. The main advantage of intermetallic compounds is the reaction capability with lithium provided by the metal elements, which leads to highly reversible capacities. However, some reports showed that these intermetallic compounds can instead activate an intercalation reaction with lithium ( $\text{Li} + \text{MSb} \rightarrow \text{LiMSb}$ , therein M = Mn, Cu, etc.) [283,284], therefore lower capacities than under conversion alloy conditions are obtained. In order to clarify this aspect, further investigations, both *in-situ* and *ex-situ*, are required.

## 5. Summary

In summary, this extended overview showed the amount of research efforts towards the development of novel active anode materials for LIBs. A bright perspective is offered by nanoscience and nanotechnology. Novel techniques and deep insight on material science have offered the opportunity to design and synthesize

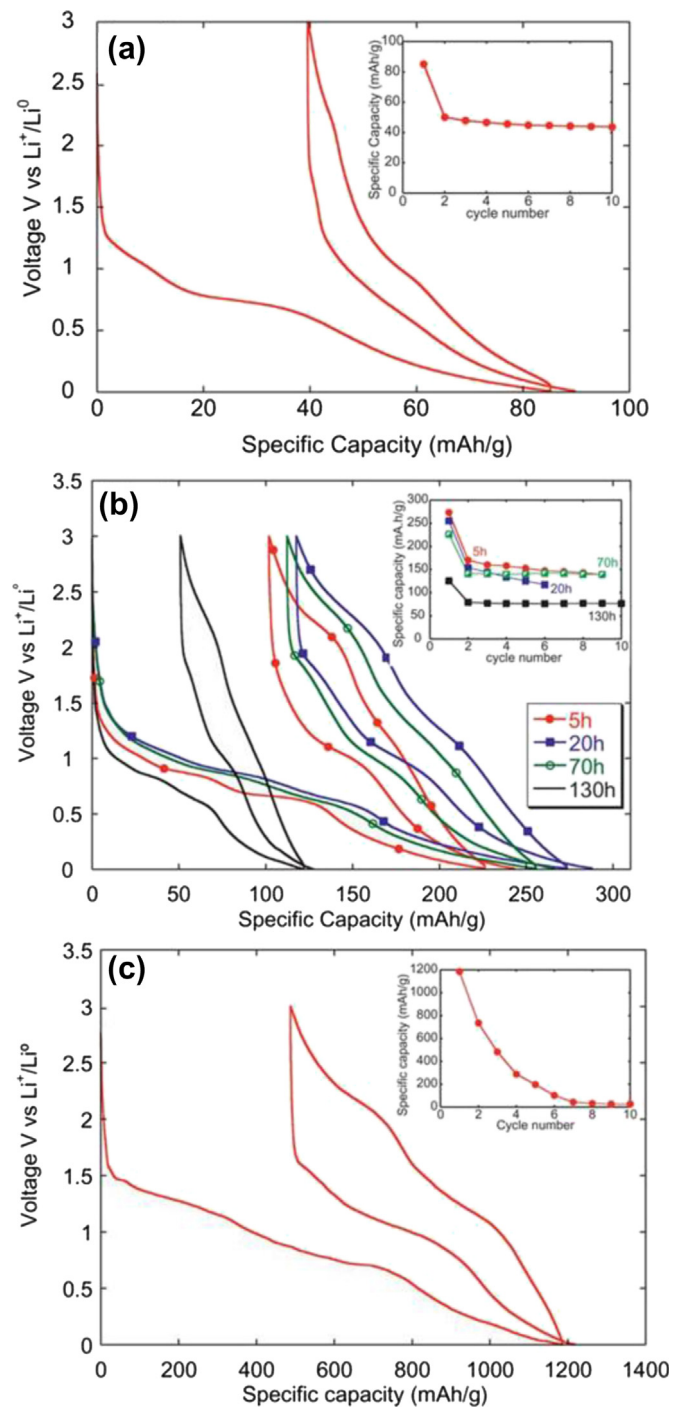


**Fig. 17.** Galvanostatic charge–discharge voltage vs. capacity curves of Ni<sub>3</sub>N prepared by (a) ammonolysis of Ni(NH<sub>3</sub>)<sub>6</sub>Br<sub>2</sub>; (b) from nickel nanoparticles with ammonia at 260 °C; (c) from decomposition of nickelamide at 150 °C for 70 h. The cells are at the rate of 1 Li per 20 h (C/20). The insets describe the capacity evolution for each cycle. (From Ref. [274].)

appropriate nanostructured anode materials for the next generation of LIBs. Uniquely tailored physico-chemical properties of nanostructures allow achieving high lithium storage, high Li-ion flux at the electrode/electrolyte interface, lower diffusion length for both Li-ions and electrons, and minimal anode volume change during the charging/discharging process. These exquisite features, when combined together, can lead to high energy density and high power density devices.

In this review, three categories of LIB anode materials were described depending on their reaction mechanism with lithium.

Firstly, the intercalation/de-intercalation group, which includes carbonaceous and titanium oxides materials, was illustrated. The storage capacity, that occurs through an intercalation path, is closely associated to the surface area, morphology, crystallinity and its orientation. Soft carbons are commonly well accepted and used in the battery industry. It was seen that Soft Carbon is quite a mature technology, while Hard Carbon may present an interesting alternative solution especially for applications requiring high capacity such as in the Electric Vehicle sector. Titanium Oxide anodes are currently under development with already some utilization in the batteries industry because, unless their poor energy density, the high reversible capacity, the high power density and the associated safety make these materials very good candidates for application in high power batteries for application in Hybrid Electric Vehicles and system that required High Power. Graphene was also extensively reviewed. In particular, it was seen that their electrical properties make this materials especially suitable for hybrid graphene/metal anodes (example graphene with SnO<sub>2</sub> and Fe2O3). CNTs were overview for their very interesting academic results, although production cost might hinder their application as anode active material in the battery industry for the next future.

In a second category, alloying materials such as Si, Ge, SiO, SnO<sub>2</sub> were described. These materials can provide larger capacities and high energy density compared to the previous group, by reacting with lithium in an alloy/de-alloy electrochemical mechanism. However, this process implies large volume expansion which results into substantial capacity loss upon cycling. The reduction from bulk dimensions to the nanoscale, along with the realization of complex structures by the combination with conductive matrices, has been proposed to overcome the above specified issues and to improve the overall anode performance. Silicon and SnO<sub>2</sub> and their composite with carbon are the most promising materials for applications in future lithium batteries, however an inexpensive way for their mass production as anode materials is still necessary. On the other hand Ge, although interesting for its electrochemical properties and excellent experimental laboratory results, suffers of the drawback of being the fiftieth ranks element in terms of abundance in the Earth's crust. Therefore, it seems not to be a good option for lithium battery technology mass application.

In the third group, materials reacting with lithium in a conversion reaction fashion were described. In particular, metal oxides/phosphides/nitrides/sulphides were considered. However, these materials are still far away from the large commercial lithium battery market, due to poor capacity retention and large potential hysteresis. Therefore, a variety of nanostructured forms of these materials have also been investigated to address the above identified problems.

Finally, from this review we can conclude that nanotechnology is definitely a formidable approach for engineering the next generation of anode materials for lithium batteries. In order to utilize the described materials as effective anodes in commercial LIBs, especially for electric vehicle applications, more research work is however required. In fact, it is necessary to achieve both higher energy and higher power density together with the developing of inexpensive fabrication processes for large scale synthesis of nanosized materials. Furthermore, the investigation of the mechanisms ruling the interaction between lithium and the nanosized forms of the described materials along with the electron transport properties at the electrode/electrolyte interface are of crucial importance for the designing of the next generation of anode active materials engineered by nanotechnology.

## References

- [1] C. Capiglia, Symposium on "Welfare Future Challenges Converging to Get over the Ditch", 11th Nov., 2011. Osaka, Japan, <http://www.hp-mctr.med.osaka-u.ac.jp/italyevent.html>.
- [2] R. Marom, S.F. Amalraj, N. Leifer, D. Jacob, D. Aurbach, *J. Mater. Chem.* 21 (2011) 9938–9954.
- [3] G.P. Gholam Abbas Nazri, *Lithium Batteries: Science and Technology*, 2003 ed., Springer, 2003.
- [4] G. Girishkumar, B. McCloskey, A.C. Luntz, S. Swanson, W. Wilcke, *J. Phys. Chem. Lett.* 1 (2010) 2193–2203.
- [5] B. Scrosati, J. Garche, *J. Power Sources* 195 (2010) 2419–2430.
- [6] M. Armand, J.M. Tarascon, *Nature* 451 (2008) 652–657.
- [7] T.-H. Kim, J.-S. Park, S.K. Chang, S. Choi, J.H. Ryu, H.-K. Song, *Adv. Energy Mater.* 2 (2012) 860–872.
- [8] J.B. Goodenough, K.-S. Park, *J. Am. Chem. Soc.* 135 (2013) 1167–1176.
- [9] V. Etacheri, R. Marom, R. Elazari, G. Salitra, D. Aurbach, *Energy Environ. Sci.* 4 (2011) 3243–3262.
- [10] M. Winter, R.J. Brodd, *Chem. Rev.* 104 (2004) 4245–4270.
- [11] F. Cheng, J. Liang, Z. Tao, J. Chen, *Adv. Mater.* 23 (2011) 1695–1715.
- [12] H. Li, Z. Wang, L. Chen, X. Huang, *Adv. Mater.* 21 (2009) 4593–4607.
- [13] J.B. Goodenough, Y. Kim, *Chem. Mater.* 22 (2009) 587–603.
- [14] J.M. Tarascon, M. Armand, *Nature* 414 (2001) 359–367.
- [15] B. Xu, D. Qian, Z. Wang, Y.S. Meng, *Mater. Sci. Eng.: R: Rep.* 73 (2012) 51–65.
- [16] J. Li, J. Klee Barillas, C. Guenther, M.A. Danzer, *J. Power Sources* 230 (2013) 244–250.
- [17] M.M. Thackeray, C. Wolverton, E.D. Isaacs, *Energy Environ. Sci.* 5 (2012) 7854–7863.
- [18] A. Manthiram, *J. Phys. Chem. Lett.* 2 (2011) 176–184.
- [19] Li Yang, Boris Ravdelb, B.L. Lucht, *Electrochem. Solid-State Lett.* 13 (2010) A95–A97.
- [20] A.V. Cresce, K. Xu, *J. Electrochem. Soc.* 158 (2011) A337–A342.
- [21] R. Dédryvère, D. Foix, S. Franger, S. Patoux, L. Daniel, D. Gonbeau, *J. Phys. Chem. C* 114 (2010) 10999–11008.
- [22] K.T. Lee, S. Jeong, J. Cho, *Acc. Chem. Res.* 5 (2012) 1161–1170.
- [23] C. Capiglia, Y. Saito, H. Kageyama, P. Mustarelli, T. Iwamoto, T. Tabuchi, H. Tukamoto, *J. Power Sources* 81–82 (1999) 859–862.
- [24] C. Capiglia, Y. Saito, H. Yamamoto, H. Kageyama, P. Mustarelli, *Electrochim. Acta* 45 (2000) 1341–1345.
- [25] C. Capiglia, Y. Saito, H. Kataoka, T. Kodama, E. Quartarone, P. Mustarelli, *Solid State Ionics* 131 (2000) 291–299.
- [26] C. Capiglia, J. Yang, N. Imanishi, A. Hirano, Y. Takeda, O. Yamamoto, *Solid State Ionics* 154–155 (2002) 7–14.
- [27] C. Capiglia, J. Yang, N. Imanishi, A. Hirano, Y. Takeda, O. Yamamoto, *J. Power Sources* 119–121 (2003) 826–832.
- [28] L. Hu, Z. Zhang, K. Amine, *J. Power Sources* 236 (2013) 175–180.
- [29] X.-G. Sun, C. Liao, N. Shao, J.R. Bell, B. Guo, H. Luo, D.-E. Jiang, S. Dai, *J. Power Sources* 237 (2013) 5–12.
- [30] E. Quartarone, P. Mustarelli, *Chem. Soc. Rev.* 40 (2011) 2525–2540.
- [31] K. Xu, *Chem. Rev.* 104 (2004) 4303–4418.
- [32] R. Borup, J. Meyers, B. Pivovar, Y.S. Kim, R. Mukundan, N. Garland, D. Myers, M. Wilson, F. Garzon, D. Wood, P. Zelenay, K. More, K. Stroh, T. Zawodzinski, J. Boncella, J.E. McGrath, M. Inaba, K. Miyatake, M. Hori, K. Ota, Z. Ogumi, S. Miyata, A. Nishikata, Z. Siroma, Y. Uchimoto, K. Yasuda, K.-i. Kimijima, N. Iwashita, *Chem. Rev.* 107 (2007) 3904–3951.
- [33] Y. Liang, Z. Tao, J. Chen, *Adv. Energy Mater.* 2 (2012) 742–769.
- [34] Z. Song, H. Zhou, *Energy Environ. Sci.* 6 (2013) 2280–2301.
- [35] S. Goriparti, M.N.K. Harish, S. Sampath, *Chem. Commun.* 49 (2013) 7234.
- [36] Z. Gong, Y. Yang, *Energy Environ. Sci.* 4 (2011) 3223–3242.
- [37] C.-C. Li, Y.-W. Wang, *J. Power Sources* 227 (2013) 204–210.
- [38] M.S. Whittingham, *Chem. Rev.* 104 (2004) 4271–4302.
- [39] K. Persson, V.A. Sethuraman, L.J. Hardwick, Y. Hinuma, Y.S. Meng, A. van der Ven, V. Srinivasan, R. Kostecki, G. Ceder, *J. Phys. Chem. Lett.* 1 (2010) 1176–1180.
- [40] N.A. Kaskhedikar, J. Maier, *Adv. Mater.* 21 (2009) 2664–2680.
- [41] J. Liu, *Adv. Funct. Mater.* 23 (2013) 924–928.
- [42] F. Orsini, A. du Pasquier, B. Beaudouin, J.M. Tarascon, M. Trentin, N. Langenhuizen, E. de Beer, P. Notten, *J. Power Sources* 81–82 (1999) 918–921.
- [43] B.J. Landi, M.J. Ganter, C.D. Cress, R.A. DiLeo, R.P. Raffaelle, *Energy Environ. Sci.* 2 (2009) 638–654.
- [44] C. Kim, K.S. Yang, M. Kojima, K. Yoshida, Y.J. Kim, Y.A. Kim, M. Endo, *Adv. Funct. Mater.* 16 (2006) 2393–2397.
- [45] J. Hou, Y. Shao, M.W. Ellis, R.B. Moore, B. Yi, *Phys. Chem. Chem. Phys.* 13 (2011) 15384–15402.
- [46] H. Zhou, S. Zhu, M. Hibino, I. Honma, M. Ichihara, *Adv. Mater.* 15 (2003) 2107–2111.
- [47] J. Yang, Y. Takeda, N. Imanishi, C. Capiglia, J.Y. Xie, O. Yamamoto, *Solid State Ionics* 152–153 (2002) 125–129.
- [48] M. Ge, J. Rong, X. Fang, C. Zhou, *Nano Lett.* 12 (2012) 2318–2323.
- [49] I.-S. Hwang, J.-C. Kim, S.-D. Seo, S. Lee, J.-H. Lee, D.-W. Kim, *Chem. Commun.* 48 (2012) 7061–7063.
- [50] K. Zhuo, M.-G. Jeong, C.-H. Chung, *J. Power Sources* 244 (2013) 601–605.
- [51] J. Jiang, Y. Li, J. Liu, X. Huang, C. Yuan, X.W. Lou, *Adv. Mater.* 24 (2012) 5166–5180.

- [52] Z. Wang, L. Zhou, X.W. Lou, *Adv. Mater.* 24 (2012) 1903–1911.
- [53] P.P. Prosin, M. Carewska, S. Loret, C. Minarini, S. Passerini, *Int. J. Inorg. Mater.* 2 (2000) 365–370.
- [54] C.-H. Lai, M.-Y. Lu, L.-J. Chen, *J. Mater. Chem.* 22 (2012) 19–30.
- [55] S. Boyanov, K. Annou, C. Villevieille, M. Pelosi, D. Zitoun, L. Monconduit, *Ionics* 14 (2008) 183–190.
- [56] L. Ji, Z. Lin, M. Alcoutabi, X. Zhang, *Energy Environ. Sci.* 4 (2011) 2682–2699.
- [57] Q. Sun, X.-Q. Zhang, F. Han, W.-C. Li, A.-H. Lu, *J. Mater. Chem.* 22 (2012) 17049–17054.
- [58] J. Chen, X.-h. Xia, J.-p. Tu, Q.-q. Xiong, Y.-X. Yu, X.-l. Wang, C.-d. Gu, *J. Mater. Chem.* 22 (2012) 15056–15061.
- [59] A. Ueda, M. Nagao, A. Inoue, A. Hayashi, Y. Seino, T. Ota, M. Tatsumisago, *J. Power Sources* 244 (2013) 597–600.
- [60] H. Hwang, H. Kim, J. Cho, *Nano Lett.* 11 (2011) 4826–4830.
- [61] P.G. Bruce, B. Scrosati, J.-M. Tarascon, *Angew. Chem. Int. Ed.* 47 (2008) 2930–2946.
- [62] Y. Wang, H. Li, P. He, E. Hosono, H. Zhou, *Nanoscale* 2 (2010) 1294–1305.
- [63] Nahong Zhao, Lijun Fu, Lichun Yang, Tao Zhang, Gaojun Wang, Y. Wu, a.T.V. Ree, *Pure Appl. Chem.* 80 (2008) 2283–2295.
- [64] L. Qiao, X. Sun, Z. Yang, X. Wang, Q. Wang, D. He, *Carbon* 54 (2013) 29–35.
- [65] F. Jiao, P.G. Bruce, *Adv. Mater.* 19 (2007) 657–660.
- [66] H. Li, H. Zhou, *Chem. Commun.* 48 (2012) 1201–1217.
- [67] Y.C. Yen, S.C. Chao, H.C. Wu, N.L. Wu, *J. Electrochem. Soc.* 156 (2009) A95–A102.
- [68] H.L. Zhang, S.H. Liu, F. Li, S. Bai, C. Liu, J. Tan, H.M. Cheng, *Carbon* 44 (2006) 2212–2218.
- [69] M. Yashio, H. Wang, K. Fukuda, T. Umeno, T. Abe, Z. Ogumi, *J. Mater. Chem.* 14 (2004) 1754–1758.
- [70] L.J. Fu, H. Liu, C. Li, Y.P. Wu, E. Rahm, R. Holze, H.Q. Wu, *Solid State Sci.* 8 (2006) 113–128.
- [71] Y.B. He, F. Ning, B. Li, Q.S. Song, W. Lv, H. Du, D. Zhai, F. Su, Q.H. Yang, F. Kang, *J. Power Sources* 202 (2012) 253–261.
- [72] S.H. Ng, J. Wang, D. Wexler, K. Konstantinov, Z.P. Guo, H.K. Liu, *Angew. Chem.* 118 (2006) 7050–7053.
- [73] G. Cui, L. Gu, L. Zhi, N. Kaskhedikar, P.A. Aken, K. Mullen, J. Maier, *Adv. Mater.* 20 (2008) 3079–3083.
- [74] T.-H. Park, J.-S. Yeo, M.-H. Seo, J. Miyawaki, I. Mochida, S.-H. Yoon, *Electrochim. Acta* 93 (2013) 236–240.
- [75] O. Haik, S. Ganin, G. Gershinsky, E. Zinigrad, B. Markovsky, D. Aurbach, I. Halalay, *J. Electrochem. Soc.* 158 (2011) A913–A923.
- [76] H. Wang, M. Yoshio, T. Abe, Z. Ogumi, *J. Electrochem. Soc.* 149 (2002) A499–A503.
- [77] H. Nakagawa, Y. Domi, T. Doi, M. Ochiai, S. Tsubouchi, T. Yamanaka, T. Abe, Z. Ogumi, *J. Power Sources* 236 (2013) 138–144.
- [78] S. Tsubouchi, Y. Domi, T. Doi, M. Ochiai, H. Nakagawa, T. Yamanaka, T. Abe, Z. Ogumi, *J. Electrochem. Soc.* 160 (2013) A575–A580.
- [79] H. Zheng, Q. Qu, L. Zhang, G. Liu, V.S. Battaglia, *RSC Adv.* 2 (2012) 4904–4912.
- [80] S.L. Candelaria, Y. Shao, W. Zhou, X. Li, J. Xiao, J.-G. Zhang, Y. Wang, J. Liu, J. Li, G. Cao, *Nano Energy* 1 (2012) 195–220.
- [81] J. Sun, H. Liu, X. Chen, D.G. Evans, W. Yang, X. Duan, *Adv. Mater.* 25 (2013) 1124.
- [82] J. Ni, Y. Huang, L. Gao, *J. Power Sources* 223 (2013) 306–311.
- [83] H. Fujimoto, K. Tokumitsu, A. Mabuchi, N. Chinnasamy, T. Kasuh, *J. Power Sources* 195 (2010) 7452–7456.
- [84] J. Yang, X.-y. Zhou, J. Li, Y.-l. Zou, J.-j. Tang, *Mater. Chem. Phys.* 135 (2012) 445–450.
- [85] C.A. Bridges, X.-G. Sun, J. Zhao, M.P. Paranthaman, S. Dai, *J. Phys. Chem. C* 116 (2012) 7701–7711.
- [86] Y. Liu, J.S. Xue, T. Zheng, J.R. Dahn, *Carbon* 34 (1996) 193–200.
- [87] J. Wang, J.-L. Liu, Y.-G. Wang, C.-X. Wang, Y.-Y. Xia, *Electrochim. Acta* 74 (2012) 1–7.
- [88] J. Hu, H. Li, X. Huang, *Solid State Ionics* 176 (2005) 1151–1159.
- [89] W. Li, M. Chen, C. Wang, *Mater. Lett.* 65 (2011) 3368–3370.
- [90] Y. Yu, C. Cui, W. Qian, Q. Xie, C. Zheng, C. Kong, F. Wei, *Asia-Pacific J. Chem. Eng.* 8 (2013) 234–245.
- [91] V. Meunier, J. Kephart, C. Roland, J. Bernholc, *Phys. Rev. Lett.* 88 (2002) 075506.
- [92] C.M. Schauerman, M.J. Ganter, G. Gaustad, C.W. Babbitt, R.P. Raffaelle, B.J. Landi, *J. Mater. Chem.* 22 (2012) 12008–12015.
- [93] K. Nishidate, M. Hasegawa, *Phys. Rev. B* 71 (2005) 245418.
- [94] J. Zhao, A. Buldum, J. Han, J. Ping Lu, *Phys. Rev. Lett.* 85 (2000) 1706–1709.
- [95] R.A. DiLeo, A. Castiglia, M.J. Ganter, R.E. Rogers, C.D. Cress, R.P. Raffaelle, B.J. Landi, *ACS Nano* 4 (2010) 6121–6131.
- [96] R. Lv, L. Zou, X. Gui, F. Kang, Y. Zhu, H. Zhu, J. Wei, J. Gu, K. Wang, D. Wu, *Chem. Commun.* (2008) 2046–2048.
- [97] J. Zhou, H. Song, B. Fu, B. Wu, X. Chen, *J. Mater. Chem.* 20 (2010) 2794–2800.
- [98] H.S. Oktaviano, K. Yamada, K. Waki, *J. Mater. Chem.* 22 (2012) 25167–25173.
- [99] C. de las Casas, W. Li, *J. Power Sources* 208 (2012) 74–85.
- [100] Y. Gu, F. Wu, Y. Wang, *Adv. Funct. Mater.* 23 (2013) 893–899.
- [101] L. Xue, G. Xu, Y. Li, S. Li, K. Fu, Q. Shi, X. Zhang, *ACS Appl. Mater. Interfaces* 5 (2012) 21–25.
- [102] T.H. Yoon, Y.J. Park, *Solid State Ionics* 225 (2012) 498–501.
- [103] Y. Wu, Y. Wei, J. Wang, K. Jiang, S. Fan, *Nano Lett.* 13 (2013) 818–823.
- [104] K. Bindumadhavan, S.K. Srivastava, S. Mahanty, *Chem. Commun.* 49 (2013) 1823–1825.
- [105] X. Huang, X. Qi, F. Boey, H. Zhang, *Chem. Soc. Rev.* 41 (2012) 666–686.
- [106] M. Liang, L. Zhi, J. Mater. Chem. 19 (2009) 5871–5878.
- [107] D.A.C. Brownson, D.K. Kampouris, C.E. Banks, *J. Power Sources* 196 (2011) 4873–4885.
- [108] Y. Liu, V.I. Artyukhov, M. Liu, A.R. Harutyunyan, B.I. Yakobson, *J. Phys. Chem. Lett.* 4 (2013) 1737–1742.
- [109] H.J. Hwang, J. Koo, M. Park, N. Park, Y. Kwon, H. Lee, *J. Phys. Chem. C* 117 (2013) 6919–6923.
- [110] D. Pan, S. Wang, B. Zhao, M. Wu, H. Zhang, Y. Wang, Z. Jiao, *Chem. Mater.* 21 (2009) 3136–3142.
- [111] P. Lian, X. Zhu, S. Liang, Z. Li, W. Yang, H. Wang, *Electrochim. Acta* 55 (2010) 3909–3914.
- [112] Z.-L. Wang, D. Xu, H.-G. Wang, Z. Wu, X.-B. Zhang, *ACS Nano* 7 (2013) 2422–2430.
- [113] T. Bhardwaj, A. Antic, B. Pavan, V. Barone, B.D. Fahlman, *J. Am. Chem. Soc.* 132 (2010) 12556–12558.
- [114] V.H. Pham, K.-H. Kim, D.-W. Jung, K. Singh, E.-S. Oh, J.S. Chung, *J. Power Sources* 244 (2013) 280–286.
- [115] X. Li, H. Song, H. Wang, Y. Zhang, K. Du, H. Li, J. Huang, *J. Appl. Electrochem.* 42 (2012) 1065–1070.
- [116] H. Xia, D. Zhu, Y. Fu, X. Wang, *Electrochim. Acta* 83 (2012) 166–174.
- [117] B.P. Vinayan, S. Ramaprabhu, *J. Mater. Chem. A* 1 (2013) 3865–3871.
- [118] B. Wang, X. Li, X. Zhang, B. Luo, M. Jin, M. Liang, S.A. Dayeh, S.T. Picraux, L. Zhi, *ACS Nano* 7 (2013) 1437–1445.
- [119] A. Hu, X. Chen, Y. Tang, Q. Tang, L. Yang, S. Zhang, *Electrochim. Commun.* 28 (2013) 139–142.
- [120] M. Wagemaker, F.M. Mulder, *Acc. Chem. Res.* 46 (2013) 1206–1215.
- [121] Z. Chen, I. Belharouak, Y.K. Sun, K. Amine, *Adv. Funct. Mater.* 23 (2013) 959–969.
- [122] Z. Hong, M. Wei, *J. Mater. Chem. A* 1 (2013) 4403–4414.
- [123] A. Moretti, G.-T. Kim, D. Bresser, K. Renger, E. Paillard, R. Marassi, M. Winter, S. Passerini, *J. Power Sources* 221 (2013) 419–426.
- [124] Y. Ren, Z. Liu, F. Pourpoint, A.R. Armstrong, C.P. Grey, P.G. Bruce, *Angew. Chem. Int. Ed.* 51 (2012) 2164–2167.
- [125] Y. Ma, G. Ji, B. Ding, J.Y. Lee, *J. Mater. Chem.* 22 (2012) 24380–24385.
- [126] L. Shen, C. Yuan, H. Luo, X. Zhang, K. Xu, Y. Xia, *J. Mater. Chem.* 20 (2010) 6998–7004.
- [127] X. Li, C. Wang, *J. Mater. Chem. A* 1 (2013) 165–182.
- [128] S.K. Martha, O. Haik, V. Borgel, E. Zinigrad, I. Exnar, T. Drezen, J.H. Miners, D. Aurbach, *J. Electrochem. Soc.* 158 (2011) A790–A797.
- [129] A. Mahmoud, J.M. Amarilla, K. Lasri, I. Saadoune, *Electrochim. Acta* 93 (2013) 163–172.
- [130] G.-N. Zhu, L. Chen, Y.-G. Wang, C.-X. Wang, R.-C. Che, Y.-Y. Xia, *Adv. Funct. Mater.* 23 (2013) 640–647.
- [131] J. Wang, X.-M. Liu, H. Yang, X.-d. Shen, *J. Alloys Compd.* 509 (2011) 712–718.
- [132] J.-Y. Lin, C.-C. Hsu, H.-P. Ho, S.-h. Wu, *Electrochim. Acta* 87 (2013) 126–132.
- [133] A.S. Prakash, P. Manikandan, K. Ramesha, M. Sathiya, J.M. Tarascon, A.K. Shukla, *Chem. Mater.* 22 (2010) 2857–2863.
- [134] L. Shen, E. Uchaker, X. Zhang, G. Cao, *Adv. Mater.* 24 (2012) 6502–6506.
- [135] X. Meng, M.N. Banis, D. Geng, X. Li, Y. Zhang, R. Li, H. Abou-Rachid, X. Sun, *Appl. Surf. Sci.* 266 (2013) 132–140.
- [136] D. Deng, M.G. Kim, J.Y. Lee, J. Cho, *Energy Environ. Sci.* 2 (2009) 818–837.
- [137] J.W. Kang, D.H. Kim, V. Matheu, J.S. Lim, J.H. Gim, J. Kim, *J. Electrochem. Soc.* 158 (2011) A59–A62.
- [138] D. Bresser, E. Paillard, E. Binetti, S. Krueger, M. Striccoli, M. Winter, S. Passerini, *J. Power Sources* 206 (2012) 301–309.
- [139] D. Dambournet, I. Belharouak, K. Amine, *Chem. Mater.* 22 (2009) 1173–1179.
- [140] X. Su, Q. Wu, X. Zhan, J. Wu, S. Wei, Z. Guo, *J. Mater. Sci.* 47 (2012) 2519–2534.
- [141] A.R. Armstrong, G. Armstrong, J. Canales, R. García, P.G. Bruce, *Adv. Mater.* 17 (2005) 862–865.
- [142] C. Jiang, I. Honma, T. Kudo, H. Zhou, *Electrochim. Solid-State Lett.* 10 (2007) A127–A129.
- [143] A.K. Rai, L.T. Anh, J. Gim, V. Matheu, J. Kang, B.J. Paul, J. Song, J. Kim, *Electrochim. Acta* 90 (2013) 112–118.
- [144] V. Gentili, S. Brutti, L.J. Hardwick, A.R. Armstrong, S. Panero, P.G. Bruce, *Chem. Mater.* 24 (2012) 4468–4476.
- [145] H. Liu, Z. Bi, X.-G. Sun, R.R. Unocic, M.P. Paranthaman, S. Dai, G.M. Brown, *Adv. Mater.* 23 (2011) 3450–3454.
- [146] W. Xu, Z. Wang, Z. Guo, Y. Liu, N. Zhou, B. Niu, Z. Shi, H. Zhang, *J. Power Sources* 232 (2013) 193–198.
- [147] S.-J. Park, Y.-J. Kim, H. Lee, *J. Power Sources* 196 (2011) 5133–5137.
- [148] J. Wang, Y. Zhou, B. Xiong, Y. Zhao, X. Huang, Z. Shao, *Electrochim. Acta* 88 (2013) 847–857.
- [149] A.L.M. Reddy, S.R. Gowda, M.M. Shajumon, P.M. Ajayan, *Adv. Mater.* 24 (2012) 5045–5064.
- [150] C.-M. Park, J.-H. Kim, H. Kim, H.-J. Sohn, *Chem. Soc. Rev.* 39 (2010) 3115–3141.
- [151] W.-J. Zhang, *J. Power Sources* 196 (2011) 13–24.
- [152] U. Kasavajjula, C. Wang, A.J. Appleby, *J. Power Sources* 163 (2007) 1003–1039.
- [153] H. Zhang, P.V. Braun, *Nano Lett.* 12 (2012) 2778–2783.

- [154] J. Gu, S.M. Collins, A.I. Carim, X. Hao, B.M. Bartlett, S. Maldonado, *Nano Lett.* 12 (2012) 4617–4623.
- [155] H. Wu, Y. Cui, *Nano Today* 7 (2012) 414–429.
- [156] J.R. Szczech, S. Jin, *Energy Environ. Sci.* 4 (2011) 56–72.
- [157] R. Teki, M.K. Datta, R. Krishnan, T.C. Parker, T.-M. Lu, P.N. Kumta, N. Koratkar, *Small* 5 (2009) 2236–2242.
- [158] A. Magasinski, P. Dixon, B. Hertzberg, A. Kvit, J. Ayala, G. Yushin, *Nat. Mater.* 9 (2010) 353–358.
- [159] R. Chandrasekaran, A. Magasinski, G. Yushin, T.F. Fuller, *J. Electrochem. Soc.* 157 (2010) A1139–A1151.
- [160] B. Key, R. Bhattacharyya, M. Morcrette, V. Seznec, J.-M. Tarascon, C.P. Grey, *J. Am. Chem. Soc.* 131 (2009) 9239–9249.
- [161] T.D. Hatchard, J.R. Dahn, *J. Electrochem. Soc.* 151 (2004) A838–A842.
- [162] S. Misra, N. Liu, J. Nelson, S.S. Hong, Y. Cui, M.F. Toney, *ACS Nano* 6 (2012) 5465–5473.
- [163] M.T. McDowell, S.W. Lee, J.T. Harris, B.A. Korgel, C. Wang, W.D. Nix, Y. Cui, *Nano Lett.* 13 (2013) 758–764.
- [164] M. Yoshio, H. Wang, K. Fukuda, T. Umeno, N. Dimov, Z. Ogumi, *J. Electrochem. Soc.* 149 (2002) A1598–A1603.
- [165] C.K. Chan, H. Peng, G. Liu, K. McIlwraith, X.F. Zhang, R.A. Huggins, Y. Cui, *Nat. Nano Sci.* 3 (2008) 31–35.
- [166] Y. Yao, K. Huo, L. Hu, N. Liu, J.J. Cha, M.T. McDowell, P.K. Chu, Y. Cui, *ACS Nano* 5 (2011) 8346–8351.
- [167] C.K. Chan, R.N. Patel, M.J. O'Connell, B.A. Korgel, Y. Cui, *ACS Nano* 4 (2010) 1443–1450.
- [168] R. Huang, X. Fan, W. Shen, J. Zhu, *Appl. Phys. Lett.* 95 (2009) 133113–133119.
- [169] Z. Wen, G. Lu, S. Mao, H. Kim, S. Cui, K. Yu, X. Huang, P.T. Hurley, O. Mao, *J. Chem. Electrochem. Commun.* 29 (2013) 67–70.
- [170] T. Song, J. Xia, J.-H. Lee, D.H. Lee, M.-S. Kwon, J.-M. Choi, J. Wu, S.K. Doo, H. Chang, W.I. Park, D.S. Zang, H. Kim, Y. Huang, K.-C. Hwang, J.A. Rogers, U. Paik, *Nano Lett.* 10 (2010) 1710–1716.
- [171] M.-H. Park, M.G. Kim, J. Joo, K. Kim, J. Kim, S. Ahn, Y. Cui, J. Cho, *Nano Lett.* 9 (2009) 3844–3847.
- [172] H. Wu, G. Chan, J.W. Choi, I. Ryu, Y. Yao, M.T. McDowell, S.W. Lee, A. Jackson, Y. Yang, L. Hu, Y. Cui, *Nat. Nano* 7 (2012) 310–315.
- [173] S.W. Hwang, J.K. Lee, W.Y. Yoon, *J. Power Sources* 244 (2013) 620–624.
- [174] K. Song, S. Yoo, K. Kang, H. Heo, Y.-M. Kang, M.-H. Jo, *J. Power Sources* 229 (2013) 229–233.
- [175] B. Liu, A. Abouimrane, Y. Ren, M. Balasubramanian, D. Wang, Z.Z. Fang, K. Amine, *Chem. Mater.* 24 (2012) 4653–4661.
- [176] Y. Yamada, Y. Iriyama, T. Abe, Z. Ogumi, *J. Electrochem. Soc.* 157 (2010) A26–A30.
- [177] Y. Hwa, C.-M. Park, H.-J. Sohn, *Meeting Abstracts*, MA2012-02, 2012, p. 913.
- [178] C.-M. Park, W. Choi, Y. Hwa, J.-H. Kim, G. Jeong, H.-J. Sohn, *J. Mater. Chem.* 20 (2010) 4854–4860.
- [179] M. Zhou, M.L. Gordin, S. Chen, T. Xu, J. Song, D. Lv, D. Wang, *Electrochem. Commun.* 28 (2013) 79–82.
- [180] G. Jeong, J.-H. Kim, Y.-U. Kim, Y.-J. Kim, *J. Mater. Chem.* 22 (2012) 7999–8004.
- [181] J.-H. Kim, H.-J. Sohn, H. Kim, G. Jeong, W. Choi, *J. Power Sources* 170 (2007) 456–459.
- [182] T. Tabuchi, H. Yasuda, M. Yamachi, *J. Power Sources* 146 (2005) 507–509.
- [183] J. Wang, H. Zhao, J. He, C. Wang, J. Wang, *J. Power Sources* 196 (2011) 4811–4815.
- [184] M. Yamada, K. Uchitomi, A. Ueda, K. Matsumoto, T. Ohzuku, *J. Power Sources* 225 (2013) 221–225.
- [185] M. Miyachi, H. Yamamoto, H. Kawai, *J. Electrochem. Soc.* 154 (2007) A376–A380.
- [186] M. Miyachi, H. Yamamoto, H. Kawai, T. Ohta, M. Shirakata, *J. Electrochem. Soc.* 152 (2005) A2089–A2091.
- [187] J.-H. Kim, C.-M. Park, H. Kim, Y.-J. Kim, H.-J. Sohn, *J. Electroanal. Chem.* 661 (2011) 245–249.
- [188] T. Kim, S. Park, S.M. Oh, *J. Electrochem. Soc.* 154 (2007) A1112–A1117.
- [189] B. Liu, A. Abouimrane, D.E. Brown, X. Zhang, Y. Ren, Z.Z. Fang, K. Amine, *J. Mater. Chem. A* 1 (2013) 4376–4382.
- [190] J.-I. Lee, S. Park, *Nano Energy* 2 (2013) 146–152.
- [191] N.G. Rudawski, B.R. Yates, M.R. Holzworth, K.S. Jones, R.G. Elliman, A.A. Volinsky, *J. Power Sources* 223 (2013) 336–340.
- [192] A.M. Chockla, K.C. Klavetter, C.B. Mullins, B.A. Korgel, *ACS Appl. Mater. Interfaces* 4 (2012) 4658–4664.
- [193] X.H. Liu, S. Huang, S.T. Picraux, J. Li, T. Zhu, J.Y. Huang, *Nano Lett.* 11 (2011) 3991–3997.
- [194] C.H. Kim, H.S. Im, Y.J. Cho, C.S. Jung, D.M. Jang, Y. Myung, H.S. Kim, S.H. Back, Y.R. Lim, C.-W. Lee, J. Park, M.S. Song, W.-I. Cho, *J. Phys. Chem. C* 116 (2012) 26190–26196.
- [195] M.-H. Park, Y. Cho, K. Kim, J. Kim, M. Liu, J. Cho, *Angew. Chem. Int. Ed.* 50 (2011) 9647–9650.
- [196] G. Cui, L. Gu, L. Zhi, N. Kaskhedikar, P.A. van Aken, K. Müllen, J. Maier, *Adv. Mater.* 20 (2008) 3079–3083.
- [197] R.A. DiLeo, S. Frisco, M.J. Ganter, R.E. Rogers, R.P. Raffaele, B.J. Landi, *J. Phys. Chem. C* 115 (2011) 22609–22614.
- [198] A.M. Chockla, M.G. Panthani, V.C. Holmberg, C.M. Hessel, D.K. Reid, T.D. Bogart, J.T. Harris, C.B. Mullins, B.A. Korgel, *J. Phys. Chem. C* 116 (2012) 11917–11923.
- [199] F.-W. Yuan, H.-J. Yang, H.-Y. Tuan, *ACS Nano* 6 (2012) 9932–9942.
- [200] J. Wang, N. Du, H. Zhang, J. Yu, D. Yang, *J. Mater. Chem.* 22 (2012) 1511–1515.
- [201] K.H. Seng, M.-h. Park, Z.P. Guo, H.K. Liu, J. Cho, *Nano Lett.* 13 (2013) 1230–1236.
- [202] H. Kim, J. Cho, *J. Mater. Chem.* 18 (2008) 771–775.
- [203] Z. Yang, G. Du, Z. Guo, X. Yu, S. Li, Z. Chen, P. Zhang, H. Liu, *Nanoscale* 2 (2010) 1011–1017.
- [204] X. Yin, L. Chen, C. Li, Q. Hao, S. Liu, Q. Li, E. Zhang, T. Wang, *Electrochim. Acta* 56 (2011) 2358–2363.
- [205] X.W. Guo, X.P. Fang, Y. Sun, L.Y. Shen, Z.X. Wang, L.Q. Chen, *J. Power Sources* 226 (2013) 75–81.
- [206] L. Noerochim, J.-Z. Wang, S.-L. Chou, H.-J. Li, H.-K. Liu, *Electrochim. Acta* 56 (2010) 314–320.
- [207] R. Ravikumar, S. Gopukumar, *Phys. Chem. Chem. Phys.* 15 (2013) 3712–3717.
- [208] Y. Jiang, T. Yuan, W. Sun, M. Yan, *ACS Appl. Mater. Interfaces* 4 (2012) 6216–6220.
- [209] D. Wang, X. Li, J. Yang, J. Wang, D. Geng, R. Li, M. Cai, T.-K. Sham, X. Sun, *Phys. Chem. Chem. Phys.* 15 (2013) 3535–3542.
- [210] M.-S. Park, G.-X. Wang, Y.-M. Kang, D. Wexler, S.-X. Dou, H.-K. Liu, *Angew. Chem.* 119 (2007) 764–767.
- [211] J. Ye, H. Zhang, R. Yang, X. Li, L. Qi, *Small* 6 (2010) 296–306.
- [212] J. Liu, Y. Li, X. Huang, R. Ding, Y. Hu, J. Jiang, L. Liao, *J. Mater. Chem.* 19 (2009) 1859–1864.
- [213] Y. Wang, H. C. Zeng, J. Y. Lee, *Adv. Mater.* 18 (2006) 645–649.
- [214] Z. Wang, D. Luan, F.Y.C. Boey, X.W. Lou, *J. Am. Chem. Soc.* 133 (2011) 4738–4741.
- [215] J.S. Chen, M.F. Ng, H.B. Wu, L. Zhang, X.W. Lou, *CrystEngComm* 14 (2012) 5133–5136.
- [216] P. Poizot, S. Laruelle, S. Gruegeon, J.-M. Tarascon, *J. Electrochem. Soc.* 149 (2002) A1212–A1217.
- [217] J.-S. Xu, Y.-J. Zhu, *ACS Appl. Mater. Interfaces* 4 (2012) 4752–4757.
- [218] B. Koo, H. Xiong, M.D. Slater, V.B. Prakapenka, M. Balasubramanian, P. Podsiadlo, C.S. Johnson, T. Rajh, E.V. Shevchenko, *Nano Lett.* 12 (2012) 2429–2435.
- [219] J. Liu, Y. Li, H. Fan, Z. Zhu, J. Jiang, R. Ding, Y. Hu, X. Huang, *Chem. Mater.* 22 (2009) 212–217.
- [220] N. Kang, J.H. Park, J. Choi, J. Jin, J. Chun, I.G. Jung, J. Jeong, J.-G. Park, S.M. Lee, H.J. Kim, S.U. Son, *Angew. Chem. Int. Ed.* 51 (2012) 6626–6630.
- [221] X.-H. Ma, X.-Y. Feng, C. Song, B.-K. Zou, C.-X. Ding, Y. Yu, C.-H. Chen, *Electrochim. Acta* 93 (2013) 131–136.
- [222] S. Mitra, P. Poizot, A. Finke, J.M. Tarascon, *Adv. Funct. Mater.* 16 (2006) 2281–2287.
- [223] X. Zhu, W. Wu, Z. Liu, L. Li, J. Hu, H. Dai, L. Ding, K. Zhou, C. Wang, X. Song, *Electrochim. Acta* 95 (2013) 24–28.
- [224] J.-K. Hwang, H.-S. Lim, Y.-K. Sun, K.-D. Suh, *J. Power Sources* 244 (2013) 538–543.
- [225] I.T. Kim, A. Magasinski, K. Jacob, G. Yushin, R. Tannenbaum, *Carbon* 52 (2013) 56–64.
- [226] B. Wang, J.S. Chen, H.B. Wu, Z. Wang, X.W. Lou, *J. Am. Chem. Soc.* 133 (2011) 17146–17148.
- [227] C. Wu, P. Yin, X. Zhu, C. OuYang, Y. Xie, *J. Phys. Chem. B* 110 (2006) 17806–17812.
- [228] T. Muraliganth, A. Vadivel Murugan, A. Manthiram, *Chem. Commun.* (2009) 7360–7362.
- [229] X. Xu, R. Cao, S. Jeong, J. Cho, *Nano Lett.* 12 (2012) 4988–4991.
- [230] H. Sohn, Z. Chen, Y.S. Jung, Q. Xiao, M. Cai, H. Wang, Y. Lu, *J. Mater. Chem. A* 1 (2013) 4539–4545.
- [231] D. Barreca, M. Cruz-Yusta, A. Gasparotto, C. Maccato, J. Morales, A. Pozza, C. Sada, L. Sanchez, E. Tondello, *J. Phys. Chem. C* 114 (2010) 10054–10060.
- [232] L. Zhang, P. Hu, X. Zhao, R. Tian, R. Zou, D. Xia, *J. Mater. Chem.* 21 (2011) 18279–18283.
- [233] L. Fei, Q. Lin, B. Yuan, M. Naeemi, Y. Xu, Y. Li, S. Deng, H. Luo, *Mater. Lett.* 98 (2013) 59–62.
- [234] W. Yuan, D. Xie, Z. Dong, Q. Su, J. Zhang, G. Du, B. Xu, *Mater. Lett.* 97 (2013) 129–132.
- [235] F. Wang, C. Lu, Y. Qin, C. Liang, M. Zhao, S. Yang, Z. Sun, X. Song, *J. Power Sources* 235 (2013) 67–73.
- [236] C.C. Li, Q.H. Li, L.B. Chen, T.H. Wang, *J. Mater. Chem.* 21 (2011) 11867–11872.
- [237] G. Binotto, D. Larcher, A.S. Prakash, R. Herrera Urbina, M.S. Hegde, J.M. Tarascon, *Chem. Mater.* 19 (2007) 3032–3040.
- [238] H. Guan, X. Wang, H. Li, C. Zhi, T. Zhai, Y. Bando, D. Golberg, *Chem. Commun.* 48 (2012) 4878–4880.
- [239] Y. Sun, X. Hu, W. Luo, Y. Huang, *J. Phys. Chem. C* 116 (2012) 20794–20799.
- [240] C. Peng, B. Chen, Y. Qin, S. Yang, C. Li, Y. Zuo, S. Liu, J. Yang, *ACS Nano* 6 (2012) 1074–1081.
- [241] Z.-S. Wu, W. Ren, L. Wen, L. Gao, J. Zhao, Z. Chen, G. Zhou, F. Li, H.-M. Cheng, *ACS Nano* 4 (2010) 3187–3194.
- [242] A. Paoletta, R. Brescia, M. Prato, M. Povia, S. Marras, L. De Trizio, A. Falqui, L. Manna, C. George, *ACS Appl. Mater. Interfaces* 5 (2013) 2745–2751.
- [243] J. Li, S. Xiong, X. Li, Y. Qian, *Nanoscale* 5 (2013) 2045–2054.
- [244] V. Aravindan, P. Suresh Kumar, J. Sundaramurthy, W.C. Ling, S. Ramakrishna, S. Madhavi, *J. Power Sources* 227 (2013) 284–290.
- [245] A. Bhaskar, M. Deepa, T. Narasinga Rao, *ACS Appl. Mater. Interfaces* 5 (2013) 2555–2566.

- [246] H. Liu, X. Du, X. Xing, G. Wang, S.Z. Qiao, *Chem. Commun.* 48 (2012) 865–867.
- [247] B. Laik, P. Poizot, J.-M. Tarascon, *J. Electrochem. Soc.* 149 (2002) A251–A255.
- [248] S. Gruegeon, S. Laruelle, R. Herrera-Urbina, L. Dupont, P. Poizot, J.-M. Tarascon, *J. Electrochem. Soc.* 148 (2001) A285–A292.
- [249] P. Poizot, S. Laruelle, S. Gruegeon, L. Dupont, J.M. Tarascon, *Nature* 407 (2000) 496–499.
- [250] V. Pralong, D.C.S. Souza, K.T. Leung, L.F. Nazar, *Electrochem. Commun.* 4 (2002) 516–520.
- [251] C. Villevieille, F. Robert, P.L. Taberna, L. Bazin, P. Simon, L. Monconduit, *J. Mater. Chem.* 18 (2008) 5956–5960.
- [252] S. Boyanov, D. Zitoun, M. Ménétrier, J.C. Jumas, M. Womes, L. Monconduit, *J. Phys. Chem. C* 113 (2009) 21441–21452.
- [253] L. Li, Y. Peng, H. Yang, *Electrochim. Acta* 95 (2013) 230–236.
- [254] M.G. Kim, J. Cho, *Adv. Funct. Mater.* 19 (2009) 1497–1514.
- [255] M.C. Stan, R. Klöpsch, A. Bhaskar, J. Li, S. Passerini, M. Winter, *Adv. Energy Mater.* 3 (2013) 231–238.
- [256] Y. Lu, J.-P. Tu, Q.-Q. Xiong, J.-Y. Xiang, Y.-J. Mai, J. Zhang, Y.-Q. Qiao, X.-L. Wang, C.-D. Gu, S.X. Mao, *Adv. Funct. Mater.* 22 (2012) 3927–3935.
- [257] A. Hayashi, A. Inoue, M. Tatsumisago, *J. Power Sources* 189 (2009) 669–671.
- [258] Y. Lu, J.P. Tu, J.Y. Xiang, X.L. Wang, J. Zhang, Y.J. Mai, S.X. Mao, *J. Phys. Chem. C* 115 (2011) 23760–23767.
- [259] D. Yang, J. Zhu, X. Rui, H. Tan, R. Cai, H.E. Hoster, D.Y.W. Yu, H.H. Hng, Q. Yan, *ACS Appl. Mater. Interfaces* 5 (2013) 1093–1099.
- [260] L. De Trizio, A. Figuerola, L. Manna, A. Genovese, C. George, R. Brescia, Z. Saghi, R. Simonutti, M. Van Huis, A. Falqui, *ACS Nano* 6 (2011) 32–41.
- [261] K. Aso, A. Hayashi, M. Tatsumisago, *Electrochim. Acta* 83 (2012) 448–453.
- [262] H. Senoh, H. Kageyama, T. Takeuchi, K. Nakanishi, T. Ohta, H. Sakaebi, M. Yao, T. Sakai, K. Yasuda, *J. Power Sources* 196 (2011) 5631–5636.
- [263] A. Paoletta, C. George, M. Povia, Y. Zhang, R. Krahne, M. Gich, A. Genovese, A. Falqui, M. Longobardi, P. Guardia, T. Pellegrino, L. Manna, *Chem. Mater.* 23 (2011) 3762–3768.
- [264] Q. Sun, W.-J. Li, Z.-W. Fu, *Solid State Sci.* 12 (2010) 397–403.
- [265] J. Cabana, C.M. Ionica-Bousquet, C.P. Grey, M.R. Palacín, *Electrochim. Commun.* 12 (2010) 315–318.
- [266] Y. Wang, J. Wu, Y. Tang, X. Lü, C. Yang, M. Qin, F. Huang, X. Li, X. Zhang, *ACS Appl. Mater. Interfaces* 4 (2012) 4246–4250.
- [267] N.H. Idris, M.M. Rahman, S.-L. Chou, J.-Z. Wang, D. Wexler, H.-K. Liu, *Electrochim. Acta* 58 (2011) 456–462.
- [268] C. Xu, Y. Zeng, X. Rui, N. Xiao, J. Zhu, W. Zhang, J. Chen, W. Liu, H. Tan, H.H. Hng, Q. Yan, *ACS Nano* 6 (2012) 4713–4721.
- [269] Y. Gu, Y. Xu, Y. Wang, *ACS Appl. Mater. Interfaces* 5 (2013) 801–806.
- [270] Z.-W. Fu, Y. Wang, X.-L. Yue, S.-L. Zhao, Q.-Z. Qin, *J. Phys. Chem. B* 108 (2004) 2236–2244.
- [271] Q. Sun, Z.-W. Fu, *Electrochim. Acta* 54 (2008) 403–409.
- [272] N. Pereira, L. Dupont, J.M. Tarascon, L.C. Klein, G.G. Amatucci, *J. Electrochem. Soc.* 150 (2003) A1273–A1280.
- [273] B. Das, M.V. Reddy, P. Malar, T. Osipowicz, G.V. Subba Rao, B.V.R. Chowdari, *Solid State Ionics* 180 (2009) 1061–1068.
- [274] F. Gillot, J. Oro-Sole, M.R. Palacin, *J. Mater. Chem.* 21 (2011) 9997–10002.
- [275] Q. Sun, Z.-W. Fu, *Electrochim. Solid-State Lett.* 10 (2007) A189–A193.
- [276] J.O. Besenhard, J. Yang, M. Winter, *J. Power Sources* 68 (1997) 87–90.
- [277] M.S. Whittingham, *Dalton Trans.* (2008) 5424–5431.
- [278] M. Winter, J.O. Besenhard, *Electrochim. Acta* 45 (1999) 31–50.
- [279] J. Wang, I.D. Raistrick, R.A. Huggins, *J. Electrochem. Soc.* 113 (1986) 457–460.
- [280] C.M. Park, H.J. Sohn, *Adv. Mater.* 22 (2010) 47.
- [281] K.C. Hewitt, L.Y. Beaulieu, J.R. Dahn, *J. Electrochem. Soc.* 148 (2001) A402–A410.
- [282] J. Yang, Y. Takeda, C. Capiglia, X.D. Liu, N. Imanishi, O. Yamamoto, *J. Power Sources* 119–121 (2003) 56–59.
- [283] C.M. Ionica, P.E. Lippens, J.O. Fourcade, J.C. Jumas, *J. Power Sources* 146 (2005) 478–481.
- [284] D. Larcher, L.Y. Beaulieu, D.D. MacNeil, J.R. Dahn, *J. Electrochem. Soc.* 147 (2000) 1658–1662.